

Electronic Thesis and Dissertation Repository

8-24-2020 2:00 PM

Yield-Stress Fluids in Confined Geometries

Thalia Magyar, *The University of Western Ontario*

Supervisor: de Bruyn, John R., *The University of Western Ontario*

Joint Supervisor: Poepping, Tamie L., *The University of Western Ontario*

A thesis submitted in partial fulfillment of the requirements for the Master of Science degree in Physics

© Thalia Magyar 2020

Follow this and additional works at: <https://ir.lib.uwo.ca/etd>



Part of the [Condensed Matter Physics Commons](#), and the [Fluid Dynamics Commons](#)

Recommended Citation

Magyar, Thalia, "Yield-Stress Fluids in Confined Geometries" (2020). *Electronic Thesis and Dissertation Repository*. 7307.

<https://ir.lib.uwo.ca/etd/7307>

This Dissertation/Thesis is brought to you for free and open access by Scholarship@Western. It has been accepted for inclusion in Electronic Thesis and Dissertation Repository by an authorized administrator of Scholarship@Western. For more information, please contact wlsadmin@uwo.ca.

Abstract

A yield-stress fluid is a material that has properties of both solids and conventional liquids that only begins to flow when subject to a finite stress. The behaviour of yield-stress fluids is interesting and important in many applications. It is expected that the rheological properties of a yield-stress fluid will change when confined to a region with a length scale comparable to the characteristic scale of its microstructure. The particle size and polydispersity of two yield-stress fluids, Carbopol and poly(*N*-isopropylacrylamide), were determined using dynamic light scattering. A rheological characterization was performed on these two yield-stress fluids. Flow of water in 1 cm long square microchannels ranging in width from 100 μm to 500 μm was simulated. Microchannels were fabricated using a soft lithography method and used in micro-particle image velocimetry experiments to visualize the confined flow of water, Carbopol, and poly(*N*-isopropylacrylamide). The flow of Carbopol and poly(*N*-isopropylacrylamide) was calculated using an equation for laminar flow of a Herschel-Bulkley fluid in a circular pipe. This analysis procedure showed that Carbopol experiences a significant increase in yield stress when confined to microchannels less than 200 μm in width. Time limitations prevented us from fully characterizing the confinement effects in these materials. Nonetheless the required experimental techniques and data analysis procedures have been substantially improved over previous work, paving the way for future research in this area.

Keywords: Rheology, microfluidics, complex fluids, yield stress, confinement, Carbopol, poly(*N*-isopropylacrylamide).

Summary for Lay Audienc

A yield-stress fluid is a material that has properties of both solids and conventional liquids that only begins to flow when subjected to a finite stress. It is expected that the properties of these yield-stress fluids with change when confined to a region on the order of its particle size. The particle size of two yield-stress fluids, Carbopol and poly(*N*-isopropylacrylamide), were determined. The flow properties of these fluids were characterized. Microchannels were fabricated and used in flow visualization experiments. Time prevented a full characterization of the confinement effects in these materials. Nonetheless the required experimental techniques and data analysis procedures have been substantially improved over previous work, paving the way for future research in this area.

Acknowledgements

I am greatly indebted to my supervisors Drs. John de Bruyn and Tamie L. Poepping for their constant advice and patience over the last two years. None of the work in this thesis would be possible without them.

I am thankful for my my advisory committee, Dr. Lyudmila Goncharova and Dr. Jeffrey Hutter for providing me with helpful advice and keeping me on track.

I give special thanks to Tim Goldhawk for his patience and assistance in the Nanofabrication Lab. I am grateful to Brian Dalrymple and Frank Vans Sas for assisting me with utmost joy. They are responsible for manufacturing my microchannel moulds. In addition, I am grateful for my collaboration with Dr. Rebecca Yardley and her help synthesizing PNIPAM.

I want to thank my parents, David and Cheryl Magyar, for their constant support and for believing in me even when I did not. I am forever appreciative of my dear friends Allison Ernst, Théa Gaudet, and Christianne Hagerman for being my support system on the good days and the bad. Without their love and support, I would not have reached this far. Finally I want to thank my fellow graduate students in the Physics and Astronomy Department for ensuring that not one day went by without laughter.

You all have contributed to my education, career, and growth, and I am forever grateful.

Contents

Abstract	i
Summary for Lay Audience	ii
Acknowledgements	iii
List of Figures	vi
List of Tables	ix
List of Abbreviations	x
1 Introduction	1
1.1 Rheology	2
1.2 Viscoelasticity	2
1.3 Rheology of yield-stress fluids	7
1.4 Thixotropy	10
1.5 Carbopol	11
1.6 Poly(<i>N</i> -isopropylacrylamide)	11
1.7 Confinement Effects	13
2 Experimental Procedures	16
2.1 Carbopol	16
2.2 PNIPAM	16
2.3 Light Scattering	17

2.4	Rheometry	18
2.5	Fabrication of Microfluidic Devices	20
2.6	Numerical Modeling	22
2.7	Particle Image Velocimetry (PIV)	22
3	Results	26
3.1	Dynamic Light Scattering	26
3.1.1	Carbopol	27
3.1.2	PNIPAM	29
3.2	Rheology	33
3.2.1	Carbopol	33
	Flow Curves	33
	Amplitude Sweeps	36
	Frequency Sweeps	38
	Creep Tests	39
3.2.2	PNIPAM	40
	Flow Curves	40
	Temperature Sweeps	41
3.3	Numerical Modeling	44
3.4	Micro-Particle Image Velocimetry	45
3.4.1	Analysis	51
4	Discussion and Conclusions	56
	Bibliography	63
A	MATLAB Codes	69
	Curriculum Vitae	89

List of Figures

1.1	A simple illustration of shear	3
1.2	Schematic of a dashpot.	4
1.3	Schematic of a linear elastic spring.	4
1.4	Schematic of the Maxwell model.	5
1.5	Schematic of the Kelvin-Voigt model.	5
1.6	Schematic of solutions to Maxwell and Kelvin-Voigt models	8
1.7	Schematic of the Herschel-Bulkley model	9
1.8	Schematic illustration of the flow curves of a thixotropic fluid.	10
1.9	Chemical structure of Carbopol	12
1.10	Schematic illustration of the structural change of PNIPAM across the LCST. . .	13
2.1	Benchtop rheometer (Anton Paar MCR302) used to to obtain the measurements in Section 3.2 [1].	19
2.2	The Plexiglas used to form the microchannels	21
2.3	Computational domain of a 500 μm channel	23
2.4	Computational mesh for water in a 500 μm channel	23
2.5	An example of a fluorescent particle image from a time series used in the PIV measurements. Lightly mixed 0.3 wt% Carbopol is flowing at 100 $\mu\text{L/hr}$ through a 500 μm channel.	25
2.6	Velocity field measured for water flowing in a 500 μm channel at 100 $\mu\text{L/hr}$. .	25
3.1	Autocorrelation function of the scattered light intensity for Carbopol from DLS	28
3.2	Distribution function of Carbopol from DLS	29

3.3	Autocorrelation function of the scattered light intensity for 10 wt% Medium BIS PNIPAM from DLS	30
3.4	Distribution function of 10 wt% Medium BIS PNIPAM from DLS	31
3.5	Medium BIS and High BIS PNIPAM raddius vs. temperature	32
3.6	Shear stress vs. shear rate of Carbopol samples fitted to the Herschel-Bulkley model	34
3.7	The storage (G') and loss modulus (G'') of Carbopol as a function of strain. . .	37
3.8	The storage (G') and loss modulus (G'') of Carbopol as a function of angular frequency.	38
3.9	Creep tests of Carbopol samples	40
3.10	Shear stress vs. shear rate of 10 wt% PNIPAM, with 3 different BIS concentrations, for 10, 20, and 30°C fitted to the Herschel-Bulkley model	41
3.11	Herschel-Bulkley parameters for 10 wt% PNIPAM, with 3 different BIS concentrations, for increasing and decreasing flow curves at temperatures ranging 5 to 35°C.	42
3.12	Viscosity of 10 wt% PNIPAM, with 3 different BIS concentrations, at a constant shear rate of 50 s ⁻¹ as a function of temperature.	43
3.13	Velocity profile from an Ansys Fluent simulation for water in a 500 μm channel	44
3.14	Velocity profile of a) water, b) vigorously mixed 0.3 wt% Carbopol, and c) 10 wt% High BIS PNIPAM in a 500 μm square channel at a flow rate of 50 μL/hr. .	45
3.15	Flow profile of vigorously mixed 0.3 wt% Carbopol flowing at 50 μL/hr in a 500 μm channel.	48
3.16	Average plug velocities of Carbopol samples in each channel at the mid-plane, approximately half way along the channel	49
3.17	Average plug velocities of PNIPAM samples in each channel at the mid-plane, approximately half way along the channel	50

3.18	Plot of equation 3.1 for vigorously mixed 0.3 wt% Carbopol flowing at 50 $\mu\text{L/hr}$ in a 500 μm channel, overlaid with the mean μPIV data	52
3.19	Logarithmic plot of flow rate versus $\sigma_w - \sigma_y$ for lightly mixed 0.14 wt% Carbopol in a 500 μm channel	53
A.1	pivplot3Davg.m GUI	69
A.2	plug.m GUI	78

List of Tables

2.1	Compositions for the synthesis of PNIPAM microgels.	17
2.2	Dimensions of the microchannels based on an average of 4 positions along the channel each.	22
3.1	Fit parameters determined by fitting the flow curves of the Carbopol samples to the Herschel-Bulkley model	35
3.2	Yield stresses obtained from flow curves and creep tests	39
3.3	Maximum velocities of water in the mid-plane approximately half way along the 1 cm long channel.	46
3.4	v_{max}/v_{avg} of water in microfluidic channels derived from v_{max} measured for μ PIV and v_{avg} calculated from the flow rate and nominal channel dimensions.	47
3.5	Width of plug averaged over flow rates displayed by Carbopol and PNIPAM samples at the mid-plane, approximately half way along the channel.	50
3.6	Yield stresses that resulted in the best fit for a logarithmic plot of $\sigma_w - \sigma_y$ vs. flow rate.	54
3.7	Inverse of slope values of a logarithmic plot of flow rate versus $\sigma_w - \sigma_y$, which is equivalent to the power law index, n	55

List of Abbreviations

DLS	Dynamic Light Scattering
LCST	Lower Critical Solution Temperature
μ PIV	micro-Particle Image Velocimetry
BIS	N,N'-methylenebisacrylamide
PIV	Particle Image Velocimetry
PDMS	Polydimethylsiloxane
PNIPAM	poly(<i>N</i> -isopropylacrylamide)
KPS	Potassium Peroxodisulfate
SDS	Sodium Dodecyl Sulfate

Chapter 1

Introduction

Imagine you're scooping a spoonful of mayonnaise from a jar. Once you remove your spoon its shape remains in the mayonnaise for a time. On the other hand, if you take a spoonful of water from a jar, the surface of the water will quickly return to being flat and uniform. Mayonnaise, peanut butter, ketchup, and many of the contents in your fridge differ from the well-known Newtonian fluids like water. These materials are referred to as complex fluids. Complex fluids have interesting and useful behaviour that is in many ways intermediate between that of solids and conventional liquids. This is a result of their microstructure. Newtonian fluids contain molecules - and nothing larger. Mayonnaise is an emulsion of oil droplets suspended in a base composed of egg yolk and lemon juice or vinegar. Its microstructure is these oil droplets. The complex fluids discussed in this thesis have a microstructure consisting of nanometer and micrometer sized polymer particles.

In some cases, a material's microstructure gives it the ability to support a finite shear stress. Such materials are known as yield-stress fluids. The behaviour of mayonnaise is a result of its yield stress. When one of these yield-stress fluids is confined to a small region with a length scale comparable to the characteristic scale of their microstructure, the material cannot be treated as a continuum in the confinement direction. It is expected that its rheological

properties will vary in this confined environment. As a result, its flow behaviour is expected to deviate from that predicted by the rheology measured on the bulk scale.

The confinement of yield-stress fluids is not fully understood. Liu, et al. have done preliminary studies of confinement effects in yield-stress fluids [2]. Their results indicated that the yield stress of Carbopol vanishes when the material is confined in two dimensions on a scale smaller than approximately 150 μm . Based on Liu's work, confinement effects are expected to become noticeable when the dimensions of the flow become comparable to the characteristic size scale of the material's microstructure. The purpose of this thesis is to investigate the effect of confinement on the flow of yield-stress fluids in more detail.

1.1 Rheology

Rheology is the science of deformation and flow of fluids [3]. Specifically, it is concerned with the properties that determine how a material will deform or flow when subjected to an external force or system of forces [4]. A common rheological test is a flow curve, in which shear stress is measured as a function of shear rate. Stress is the force per unit area applied to a material, $\sigma = \frac{F}{A}$. Shear is a sliding deformation that occurs when there is movement between layers of a sample. Consider a slab of material sheared between two parallel plates as seen in Figure 1.1. Shear is created by applying external forces in the planes of the top and bottom plates and the resulting shear strain is calculated from the deformation of the material. Strain, $\gamma = \frac{\Delta x}{h}$, is the relative deformation of the fluid; the displacement of an element of fluid divided by the height of the slab. The shear rate, $\dot{\gamma}$, is the first derivative of the strain with respect to time.

1.2 Viscoelasticity

Newtonian liquids, like water and alcohol, flow in response to any given stress. A Newtonian fluid is characterized by a viscosity that is independent of shear stress, shear rate, and flow

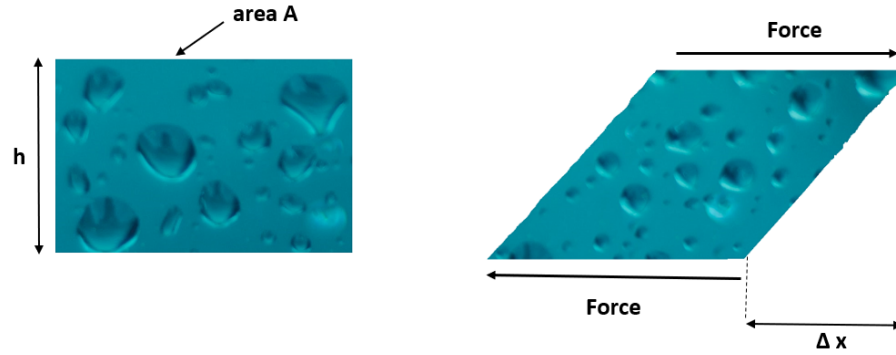


Figure 1.1: A simple illustration of shear. A force F applied parallel to a slab of height h , over an area A , results in a shear stress $\sigma = F/A$, and creates a deformation along the x direction of Δx , which results in a shear strain $\gamma = \Delta x/h$.

history at a fixed temperature. The viscosity, η , is defined by Newton's law of viscosity:

$$\sigma = \eta \dot{\gamma}. \quad (1.1)$$

When a purely viscous fluid is subjected to an applied stress, the strain increases linearly for as long as the stress is applied. When the stress is removed, the strain remains and the fluid does not relax [5].

Solids, on the other hand, respond elastically to a small applied force. The elasticity of the material describes its ability to deform reversibly when subjected to an applied force. For small shear forces, Hooke's law applies:

$$\sigma = G\gamma, \quad (1.2)$$

where σ is the shear stress, G is the elastic constant, and γ is the strain. When an elastic material is subjected to a stress it maintains the resulting elastic strain for as long as the stress is applied. When the stress is removed, the strain instantaneously vanishes [5].

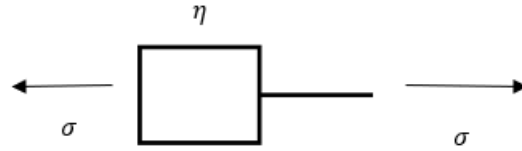


Figure 1.2: Schematic of a dashpot.

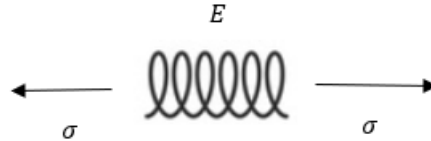


Figure 1.3: Schematic of a linear elastic spring.

Complex fluids possess mechanical properties that are intermediate to ordinary liquids and solids. Solids deform in response to stress, and liquids flow. Many complex fluids will maintain their shape on short time scales and flow on long time scales. This property is known as viscoelasticity [6]. When you throw silly putty against a wall, the time scale is short and the putty behaves elastically, bouncing like a rubber ball. On the other hand, when silly putty is slowly stretched it behaves viscously and flows irreversibly. Silly putty is viscoelastic as are thousands of other materials including nylon, human tissue, and lava [7].

Complex fluids display a combination of viscous and elastic behaviour, and can be described by combining Newton's law of viscosity and Hooke's law. Conceptually, the viscous component of a complex fluid's behaviour can be represented by a viscous dashpot, Figure 1.2, and the elastic component by an elastic spring, Figure 1.3.

A dashpot is a piston-cylinder arrangement filled with a viscous fluid. A viscous dashpot responds to an applied stress with a strain rate proportional to that stress,

$$\dot{\gamma} = \frac{1}{\eta}\sigma. \quad (1.3)$$

For a linear elastic spring of stiffness E , on the other hand,

$$\gamma = \frac{1}{E}\sigma. \quad (1.4)$$

In this case, it is the strain that is proportional to the applied stress.

Just as resistors and inductors can be connected in series and in parallel to form electric circuits, the spring and the dashpot can be connected in series and in parallel to model viscoelastic behaviour [8]. The Maxwell model connects the spring and dashpot in series, as shown in Figure 1.4, and the Kelvin-Voigt model connects them in parallel as shown in Figure 1.5.

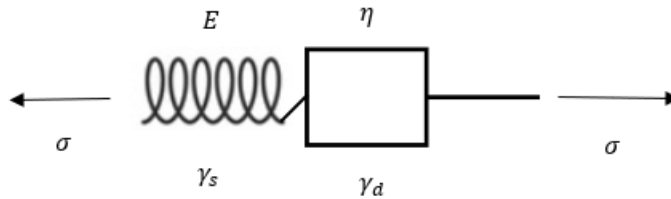


Figure 1.4: Schematic of the Maxwell model.

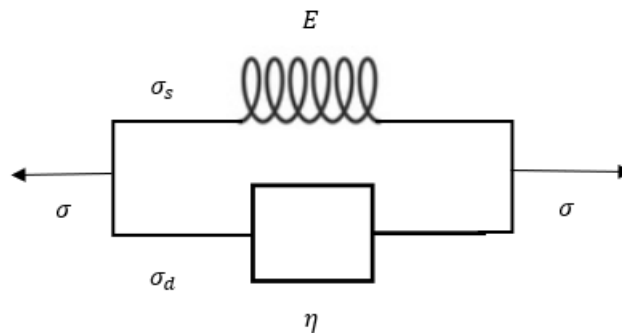


Figure 1.5: Schematic of the Kelvin-Voigt model.

In the Maxwell model, one can divide the total strain on the spring-dashpot combination into

the elastic strain of the spring, γ_s , and the viscous strain of the dashpot, γ_d . Equilibrium requires that the stress be the same in both elements leading to the following three equations:

$$\begin{aligned}\gamma_s &= \frac{1}{E}\sigma \\ \dot{\gamma}_d &= \frac{1}{\eta}\sigma\end{aligned}\tag{1.5}$$

$$\gamma = \gamma_s + \gamma_d.$$

Combining these equations gives a differential equation for the stress in the Maxwell model,

$$\sigma + \frac{\eta}{E}\dot{\sigma} = \eta\dot{\gamma}.\tag{1.6}$$

When the Maxwell model is subjected to a stress, the spring will stretch immediately while the dashpot will deform at a steady rate. When the stress is removed, the spring again reacts immediately, but the viscous strain in the dashpot does not tend to recover [5].

The Kelvin-Voigt model consists of a spring and a dashpot in parallel. In this case, the strain is the same across both elements, and the stress is the sum of the viscous stress on the dashpot and the elastic stress on the spring. Analyzing this system gives the following equations:

$$\begin{aligned}\gamma &= \frac{1}{E}\sigma_s \\ \dot{\gamma} &= \frac{1}{\eta}\sigma_d\end{aligned}\tag{1.7}$$

$$\sigma = \sigma_s + \sigma_d.$$

Rearranging these equations gives the constitutive law for the Kelvin-Voigt model,

$$\sigma = E\gamma + \eta\dot{\gamma}\tag{1.8}$$

[8].

When a stress is applied to the Kelvin-Voigt model, the spring will want to stretch, but it will be held back by the dashpot, which cannot react immediately. The stress is initially all in the dashpot and over time is transferred to the spring. When the stress is removed, the spring will want to contract, but once again the dashpot holds it back. In time, the spring will eventually pull the dashpot back to its original zero position and fully recover [5].

Both models are necessary for describing the behaviour of yield-stress fluids. Although real fluids tend to be more complex than these models, they are a great tool for beginning to understand the behaviour of yield-stress fluids. Figure 1.6 shows schematic solutions to Maxwell and Kelvin-Voigt models for stress relaxation and creep tests. The Maxwell model is good at describing the relaxation behaviour after a stress load is removed. The Kelvin-Voigt model predicts creep, to be explained below, more realistically than the Maxwell model.

1.3 Rheology of yield-stress fluids

Imagine squeezing toothpaste out of a tube. When you open the tube and turn it upside down the toothpaste does not flow. Once you squeeze the tube hard enough, however, the toothpaste flows. This is because toothpaste has a yield stress. When the applied shear stress is smaller than the yield stress, σ_y , the toothpaste behaves like a solid and does not flow. For stresses larger than the yield stress, it flows like a viscous liquid.

For Newtonian fluids, stress is proportional shear rate. Yield-stress fluids, in contrast, are commonly described using the Herschel-Bulkley model,

$$\begin{cases} \sigma = \sigma_y + k\dot{\gamma}^n & \sigma > \sigma_y \\ \dot{\gamma} = 0 & \sigma \leq \sigma_y \end{cases}$$

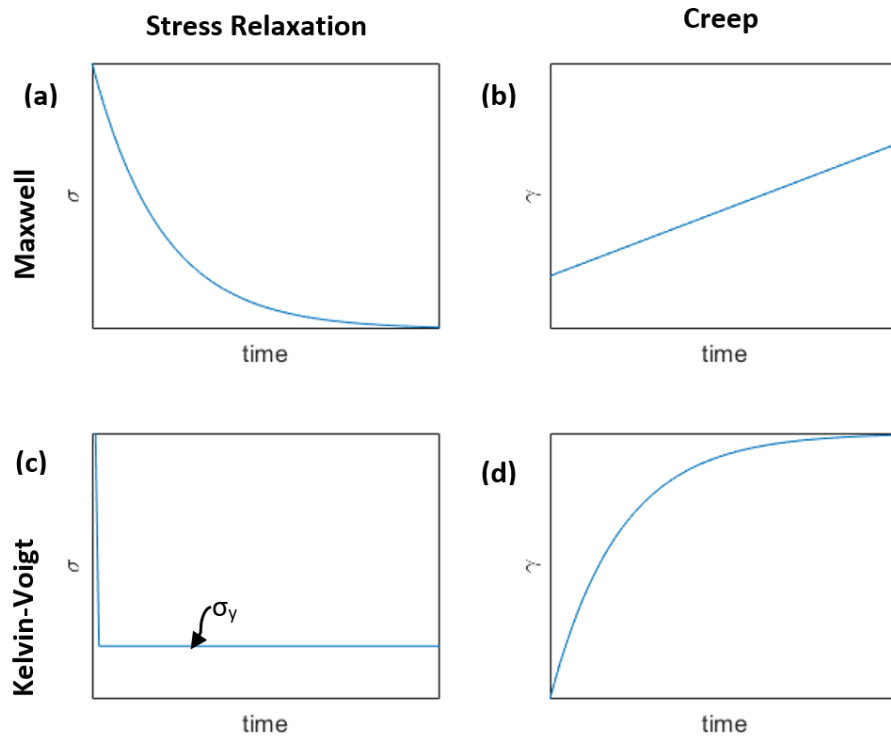


Figure 1.6: Schematic of solutions to Maxwell and Kelvin-Voigt models. a) Stress relaxation function for the Maxwell model. b) Creep for the Maxwell model. c) Stress relaxation function for the Kelvin-Voigt model. d) Creep for the Kelvin-Voigt model.

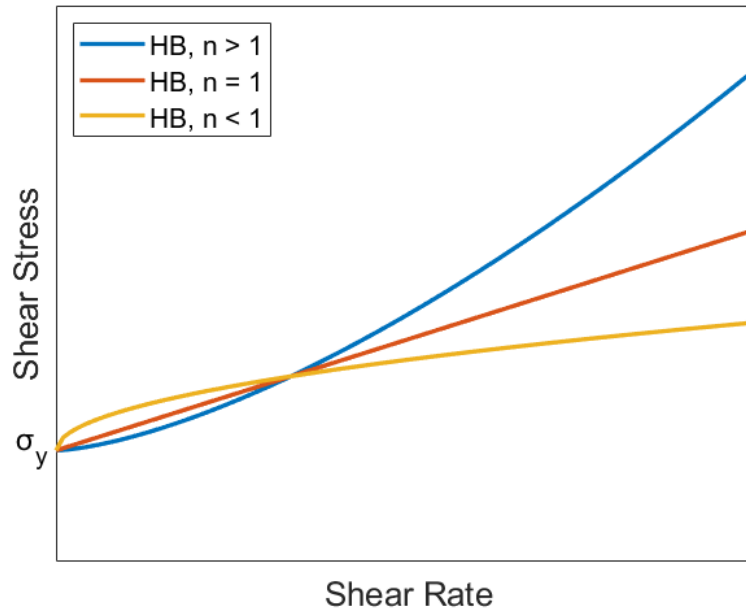


Figure 1.7: Schematic of the Herschel-Bulkley model. The fluid is shear thickening when $n > 1$, shear thinning when $n < 1$, and Bingham when $n = 1$.

where k is the consistency index and n is the power index. The Herschel-Bulkley model describes a non-thixotropic yield-stress fluid in which the viscous contribution is non-linear. The influence of the power index is displayed in Figure 1.7. When n is greater than one, the fluid is shear thickening, meaning that once the yield stress is surpassed it begins to flow and becomes more viscous as shear rate is increased. When n is less than one the fluid is shear thinning. A shear thinning fluid, just like a shear thickening one, begins to flow once the yield stress is surpassed but becomes less viscous as shear rate is increased. When $n = 1$ the fluid is referred to as a Bingham fluid and displays both a linear relationship between stress and shear rate and a yield stress.

There are a number of ways of measuring the yield stress of a material. The classical way, and the way used in this thesis, is to measure shear stress as a function of shear rate and fit the data to the Herschel-Bulkley model.

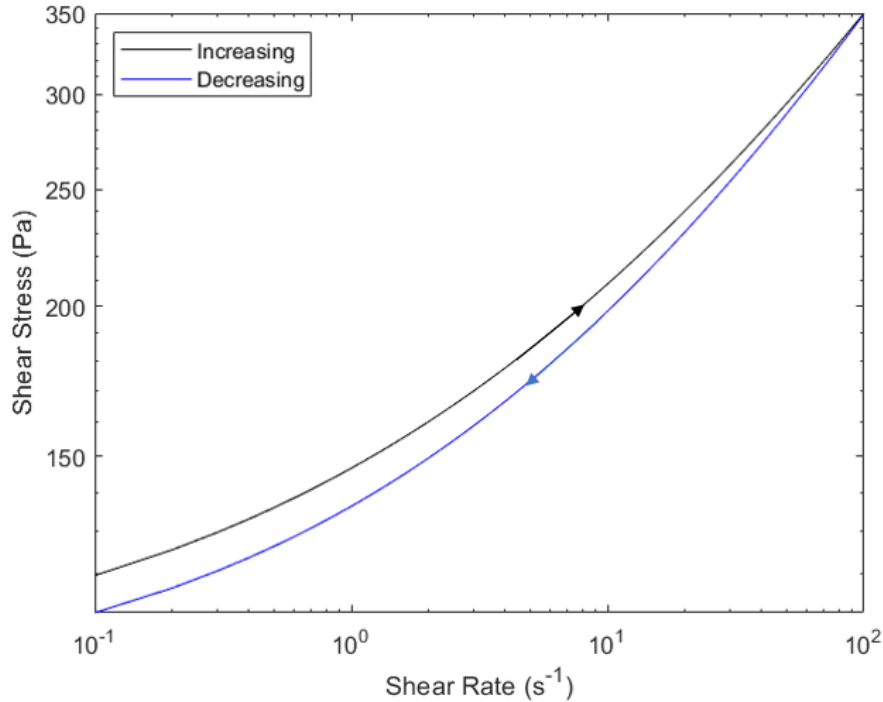


Figure 1.8: Schematic flow curves of a thixotropic fluid measured by first increasing, then decreasing the shear rate.

1.4 Thixotropy

Figure 1.8 shows schematic flow curves of a thixotropic fluid, measured first by increasing the shear rate, and then by decreasing it. Thixotropy is revealed by the hysteresis between the two curves. In thixotropic fluids, like ketchup and paint [9], the rate at which the microstructure recovers after being disrupted by shear is slower than the rate of the shear itself. This implies that after a change in shear rate there is an equilibration time over which the fluid properties adjust. The amount of thixotropy depends on the rate at which the shear rate changes. When the shear rate is increased slowly, there is less hysteresis because the fluid properties have more time to adjust to the conditions.

1.5 Carbopol

Carbopol is a family of commercial polymers frequently employed in the cosmetics, pharmaceutical, paint, and food industries as a thickening, suspending, dispersing, or stabilizing agent [10, 11]. Carbopol is transparent, easy to prepare, displays a yield stress, and is insensitive to temperature, making it ideal for a wide variety of rheological studies [10, 12, 13]. Its properties are tunable by varying concentration and pH . Carbopol is made up of particles of modified cross-linked poly(acrylic acid), as shown in Figure 1.9. When dry, the polymer particles are 0.2 μm in average diameter and form a fluffy white powder [14]. When dispersed in water and pH -neutralized, the particles swell up to 1000 times their former volume [12, 15]. Unmodified, Carbopol has a pH of approximately 3. A neutralizing agent, commonly sodium hydroxide, is added to increase the pH . When neutralized, the osmotic pressure of the sodium ions causes the cross-linked polymer network to swell, creating what is known as a polymer microgel.

1.6 Poly(*N*-isopropylacrylamide)

Poly(*N*-isopropylacrylamide) (PNIPAM) is a transparent intramolecularly cross-linked microgel. PNIPAM is made by crosslinking a monomer, *N*-isopropylacrylamide (NIPAM), with *N,N'*-methylenebisacrylamide (BIS) using emulsion polymerization [16]. The resulting powder is dissolved in distilled water to form a solution of nanometer sized spherical microgel particles. PNIPAM is a thermosensitive yield-stress fluid. As temperature increases the microgel particles decrease in size, and the effective particle volume fraction decreases [17]. When the solution is heated above the lower critical solution temperature (LCST), which is approximately 32°C - 33°C [16–19], PNIPAM shows a reversible chain collapse as it becomes thermodynamically more favourable for the polymer to associate with itself than with water. This means that PNIPAM chains dissolved in the solution will spontaneously phase separate as temperature increases beyond the LCST.

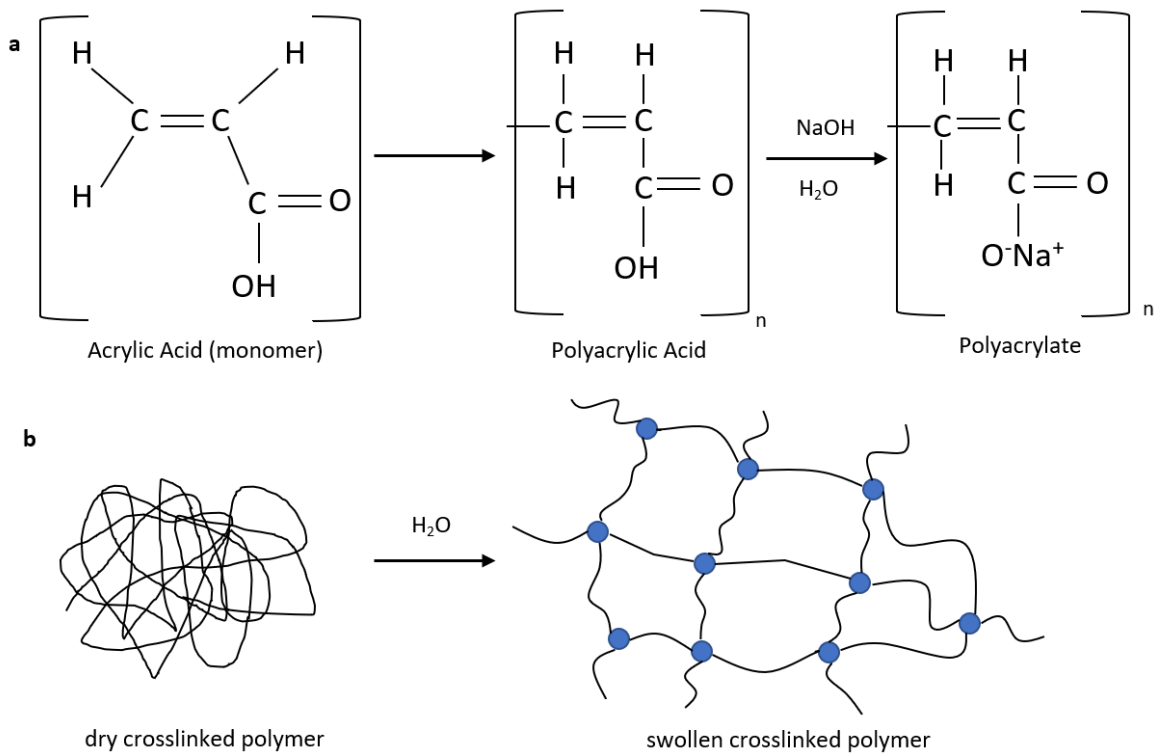


Figure 1.9: a) The chemical reaction of poly(acrylic acid) with a neutralizing agent such as sodium hydroxide. b) Crosslinkers are added to form a network of polymer chains interconnected via cross-linking. This dry cross-linked polymer gets hydrated and swells.

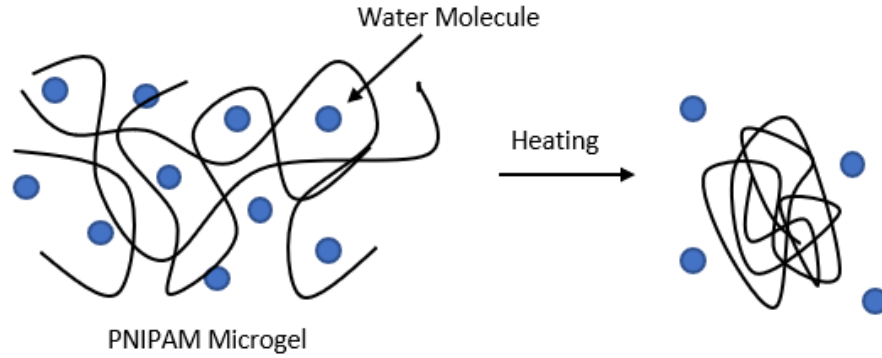


Figure 1.10: Schematic illustration of the structural change of PNIPAM across the LCST. The blue circles are representative of water molecules and the black lines are representative of the PNIPAM polymer chains. The right hand side of the figure showcases how water is expelled outside of the PNIPAM chains when temperature is heated to the LCST or beyond.

1.7 Confinement Effects

When a complex fluid is confined to a geometry with a length scale comparable to the material's microstructure, the material can no longer be treated as a continuum in the confinement direction and the details of its microstructure become important. As a result, its flow behaviour is expected to deviate from that predicted based on the rheology measured on the bulk scale.

Jofore, et al. measured the flow curve of three concentrations of Carbopol in a flexure-based micro-gap rheometer with a gap ranging 5 to 100 μm . At large gaps all three concentrations generally agreed with the bulk data. When the width of the shearing gap was reduced to a value on the order of the average dimension of a particle, the yield stress was increased by a factor of 4 [20].

Yan, et al. measured the flow curve of Carbopol using squeeze flow rheometry. They found that the flow properties began to differ significantly from the bulk rheology measurements at a

gap of 200 μm , one to two orders of magnitude larger than the particle size. They observed a significant increase in yield stress here. After the transition, however, the yield stress gradually decreased with decreasing separation, but was still greater than the bulk yield stress at the smallest gap of 70 μm [21].

Geraud, et al. used parallel-plate rheometry to study the flow properties of Carbopol for different gap sizes. They saw an increase in yield stress when the gap was decreased to approximately 500 μm . In addition, they studied the flow of Carbopol in a glass channel 1 mm x 116 μm x 45 mm in size at pressures ranging from 0.15 bar to 1 bar. The resulting maximum velocity was 60-70% higher than expected based on the bulk rheology [13], suggesting an increase in wall slip and/or a decrease in the yield stress.

Liu, et al. studied the confinement of Carbopol in square microchannels ranging from 50 μm to 500 μm in width. In larger channels, the velocity profiles agreed well with predictions based on the bulk rheology of Carbopol, and no effects of confinement were observed. In smaller channels, however, the velocity profiles deviated substantially from the bulk-scale predictions and could not be fitted by a model with a yield stress [2, 22]. These results indicated that the yield stress of Carbopol vanishes when the material is confined in two dimensions on a scale smaller than approximately 150 μm , which is about 3 times the maximum particle size for Carbopol found by Lee, et al [12].

It has recently been demonstrated that the size and polydispersity of the particles in a Carbopol solution depend on the amount of shear applied during mixing and that this in turn affects the rheology of the fluid [23]. The yield stress and viscosity decrease with increased stirring time and a hysteresis loop becomes more pronounced. Dinkgreve states “the extent of the hysteresis loop depends exactly on the type of stirrer, its size, the volume of the container with respect to the stirred region, etc.; it is therefore very difficult to perform a systematic study on the effect

of stirring” [23].

We expect confinement effects to become important when the dimensions of the flow channel become comparable to the characteristic scale of the material’s microstructure. For this reason, it is important that we characterize the microstructure of our Carbopol samples at the same time that we study their flow behaviour; this was not done in the study of Liu, et al. [2,22]. For this reason, this thesis explores the effects of confinement on the flow behaviour of Carbopol while characterizing its microstructure. In addition, PNIPAM is studied in the same form as a control experiment. Because PNIPAM has a particle size significantly smaller than Carbopol, it is not expected to show confinement effects in the channels used. In this case, the results would further support the argument that the onset of confinement effects are correlated to particle size.

Chapter 2

Experimental Procedures

2.1 Carbopol

Carbopol solutions were prepared by dispersing a measured amount of dry Carbopol 940 (Lubrizol) powder in deionized water at room temperature while stirring with a propeller-blade mixer at 250 rpm for 24 hours to ensure it was completely dissolved. When the powder was initially dissolved in water, the solution had a pH of approximately 3. A benchtop pH meter (Fisher Scientific Accumet AE150) was used to monitor the pH as 25% NaOH was added, while mixing, to raise the pH to 6.00 ± 0.01 , resulting in the expansion of the microgel particles and the formation of a stiff gel. The stirring was continued for an additional 24 hours to prepare what are referred to below as “vigorously” mixed samples and 1 hour for “lightly” mixed samples. $0.52 \mu\text{m}$ fluorescent microsphere particles (ThermoScientific) were mixed by hand into the solution at an approximate volume fraction of 0.3% to serve as tracer particles in the flow velocimetry experiments described below.

2.2 PNIPAM

PNIPAM was synthesized using the method described in [16]. The components, *N*-isopropylacrylamide (NIPAM), *N,N'*-methylenebisacrylamide (BIS), potassium peroxydisulfate (KPS), and sodium

Table 2.1: Compositions for the synthesis of PNIPAM microgels.

Sample	NIPAM (g)	BIS (g)	SDS (g)	K ₂ S ₂ O ₈ (g)
Low BIS	7.85	0.065	0.15	0.32
Medium BIS	7.87	0.15	0.15	0.30
High BIS	7.89	0.57	0.16	0.33

dodecyl sulfate (SDS) were all obtained from Alfa Aesar. Emulsion polymerization was done in a 2 L three-necked flask equipped with a stirrer, a reflux condenser, and a gas inlet. The amounts of NIPAM, BIS, and SDS given in Table 2.1 were dissolved in 450 ml of Milli-Q water under stirring. The initiator KPS was dissolved in 50 ml of water. Both solutions were bubbled with nitrogen for 30 minutes. After heating the NIPAM mixture to 70°C, the initiator solution was added. Polymerization took place for 8 hours while the mixture was stirred at 300 rpm using a magnetic stir plate. The resulting dispersion was cooled to room temperature and filtered through glass wool. Further purification was done by extensive dialysis against water three times until a conductivity meter measured 1 $\mu\text{S}/\text{cm}$. The polymers were isolated by freeze-drying to form a white powder which was stored in glass jars until needed. To prepare solutions for use in our experiments, a measured amount of dried PNIPAM was dispersed in deionized water at room temperature while stirring with a magnetic stir bar at 72 rpm until fully dissolved. Fluorescent microsphere particles (0.52 μm) were mixed by hand into the solution at an approximate volume fraction of 0.3% to serve as tracer particles in the flow visualization experiments described below.

2.3 Light Scattering

Dynamic light scattering is a technique used to determine the size distribution of small particles in suspension or polymers in solution. The ALV / CGS-3 compact goniometer used in this work is a self-contained system with 22 mW helium-neon laser, ALV-proprietary optical fiber based

detector, APD-based single photon detector, ALV/LSE-5003 electronics and ALV-5000/EPP correlator [24]. Using this instrument, the size distribution of dissolved Carbopol and PNIPAM particles was measured by scattering light at an angle of 30° . A circulating water bath was used to control the temperature. The ALV system outputs the intensity autocorrelation function of the scattered light as a function of delay time. The size distribution of the suspended particles was calculated from this using a regularized inverse Laplace transform method [25, 26] based on the MATLAB function RILT [27].

2.4 Rheometry

The viscous and elastic properties of fluids and soft solids can be measured using a rheometer. In this work, an Anton Paar MCR302 rotational shear rheometer, Figure 2.1, was used to measure the rheological properties of the Carbopol and PNIPAM solutions without tracer particles at 20°C . This is a strain-controlled rheometer, which works by confining a fluid within a geometry, applying a strain, and measuring the resulting stress. The measuring geometry was a cone-and-plate with a 50 mm diameter and 4° cone angle. 600-grit sandpaper was affixed to the surfaces of both the cone and the plate with double-sided tape to minimize wall slip. An environmental housing with an atmosphere saturated with water vapour surrounded the tool to minimize evaporation over the duration of the measurements.

Viscosity was determined from measurements of shear stress as a function of shear rate. At 20°C , shear rate was increased in logarithmically spaced steps from 0.01 s^{-1} to 100 s^{-1} . After each step, the shear stress was measured after a wait time long enough that the fluid properties have time to reach a steady state. We used wait times ranging from 180 s at low shear rates to 10 s at high shear rates. From there, viscosity was determined using the ratio of shear stress over shear rate, $\eta = \frac{\sigma}{\dot{\gamma}}$.



Figure 2.1: Benchtop rheometer (Anton Paar MCR302) used to to obtain the measurements in Section 3.2 [1].

The viscous and elastic moduli, G'' and G' respectively, were determined using small-amplitude oscillatory shear measurements. An amplitude sweep was performed by applying a sinusoidally varying strain at a constant frequency of 1 s^{-1} as the strain amplitude was increased from 0.01% to 1000%. This measurement determines the fluid's linear viscoelastic regime, in which the moduli are independent of the strain amplitude. The linear viscoelastic regime indicates the range in which oscillatory strain can be applied without destroying the microscopic structure of the sample. A strain within this regime was used for measurements of the moduli as a function of frequency.

A frequency sweep was then performed using a strain amplitude within the viscoelastic regime. A strain amplitude of 1% was used for lightly mixed Carbopol samples and a strain amplitude of 0.2% was used for vigorously mixed Carbopol samples. The storage and loss modulus were measured while increasing angular frequency in logarithmically spaced steps from 0.1 to 100 s^{-1} .

The final test performed to characterize Carbopol and PNIPAM was a creep test. A constant stress was applied to the fluid for 333 s followed by a constant stress of 0 Pa for another 333 s. The resulting strain was measured as a function of time. When a constant stress is applied to a sample, the strain increases. For an elastic solid, the strain reaches a constant value. For a viscous liquid, the strain increases linearly with time. When the applied stress is removed, the elastic part of the strain recovers, but the viscous part does not. A creep test can be used to determine the yield stress of a material. The yield stress will lie somewhere between the highest applied stress that shows solid behaviour and the lowest applied stress that shows liquid behaviour.

2.5 Fabrication of Microfluidic Devices

Square microchannels 1 cm in length were fabricated from an acrylic mould using polydimethylsiloxane (PDMS, SYLGARD 184 silicone elastomer, Dow Chemical Co.). The mould was designed with SolidWorks, a 3D CAD software [28], by The University of Western Ontario's Physics and Astronomy machine shop. The CAD file was then uploaded using a tool-path generating software, Mastercam [29], to a micro mill. Using this file, the mould was machined from a piece of acrylic. Each mould incorporated three independent straight microchannels with independent inlets and outlets as shown in Figure 2.2.

PDMS base was mixed with a cross-linker in a 10:1 ratio, then degassed in a vacuum chamber. The mould was mounted in a plexiglass cylinder, the degassed PDMS was cast onto the mould, degassed a second time, and allowed to cure at room temperature. After 48 hours, the PDMS chamber was fully cured. The mould and PDMS chamber were removed from the cylinder by screwing a screw into a threaded hole at the bottom of the cylinder to push the mould out of the cylinder. The PDMS chamber was gently peeled away from the mould until it was completely removed. The chamber was then placed on the sticky side of a length of packing tape to main-

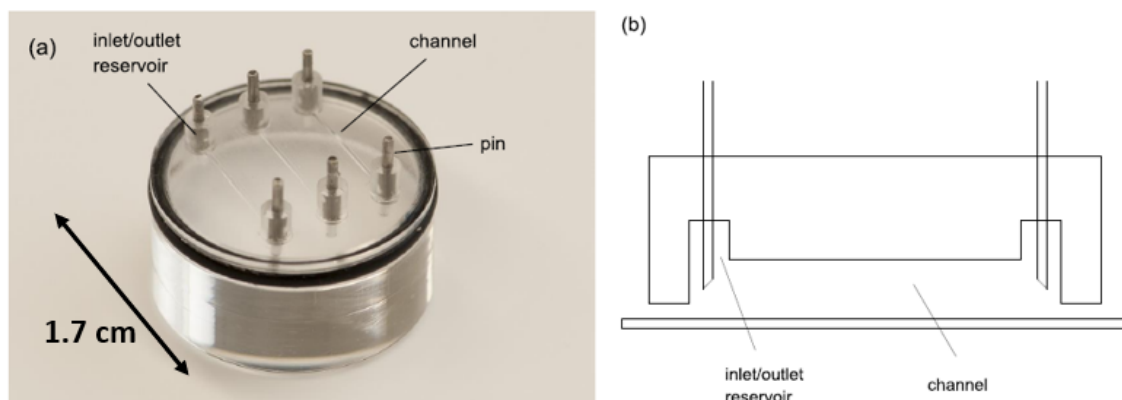


Figure 2.2: (a) The Plexiglas mould used to form the microchannels. The diameter of the mould is 1.7 cm. (b) The PDMS that was cast into the mould shown in (a) is bonded to a 5 cm glass-bottom culture dish with a partially cured layer of PDMS, and polyethylene tubes are inserted into the inlet and outlet reservoirs to form the full microchannel assembly [22].

tain a clean surface during storage.

The bottom of the channels were made by spin-coating PDMS to the bottom of a 5 cm glass-bottom culture dish (MatTek Corporation, Part No. P50G-0-30-F) for 10 seconds at 500 rpm followed by 60 seconds at 3000 rpm. The coated culture dish was placed in a microwave beside a beaker of 400 ml of water and partially cured for 20-22 minutes at 540 W. The PDMS chamber was then removed from the packing tape and lightly pressed into the partially cured PDMS layer on the dish. Air bubbles were removed by pressing gently on the top chamber, working from the centre of the device outwards. To irreversibly bond the chamber to the PDMS-coated glass substrate, the assembly was left at room temperature for 24 hours to allow the PDMS to fully cure. 23.5 gauge needles (outer diameter of 0.59 mm) were attached to teflon tubing with an inner diameter of 0.56 mm and an outer diameter of 1.1 mm. The tubing was inserted into the inlets and outlets of the channels, and bonded using Lepage 5 minute epoxy.

Four different sizes of microchannels, ranging in width from 100 μm to 500 μm , were used in our experiments. All channels were 1 cm in length. The actual dimensions of the channels

Table 2.2: Dimensions of the microchannels based on an average of 4 positions along the channel each.

mold width (μm)	500	300	200	100
channel width (μm)	564 ± 5	293 ± 4	137 ± 2	68 ± 1
channel height (μm)	572 ± 3	258 ± 4	177 ± 2	103 ± 3

were slightly different than those of the positive mould, and were determined from measurements made with an inverted microscope (Olympus IX71) with a 40 \times objective (20 \times for the 500 μm channel), at four positions along the length of the channels. The mean and standard deviation of these measurements are shown in Table 2.2.

2.6 Numerical Modeling

Ansys Fluent software [30] was used to simulate the flow of water in microchannels, and to predict the velocity profiles in the channels. A density of 1 $\text{g}\cdot\text{ml}^{-1}$ and a constant viscosity of 1.003 $\text{mPa}\cdot\text{s}$ was used. Figure 2.3 displays the computational domain used to simulate the 500 μm channel. Since a parabolic flow profile is expected for water, a uniform square mesh was used with 200 nodes along the 1 cm channel length and 25 nodes across the channel width for the 500 μm channel, 20 nodes across the channel width for the 300 and 200 μm channels, and 15 nodes across the channel width for the 100 μm channel.

2.7 Particle Image Velocimetry (PIV)

Particle image velocimetry (PIV) is a non-intrusive laser optical measurement technique that determines the velocity field of a flowing fluid by tracking the motion of tracer particles suspended in the flow. In this work, micro-PIV (μPIV) was used to measure the velocity fields of our experimental fluid flowing in the microchannels, which were mounted on an Olympus

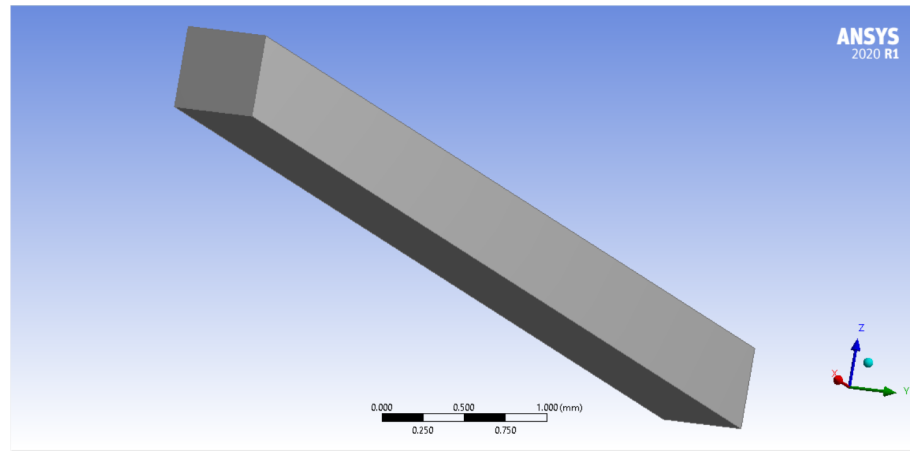


Figure 2.3: Computational domain used to simulate the 500 μm channel.

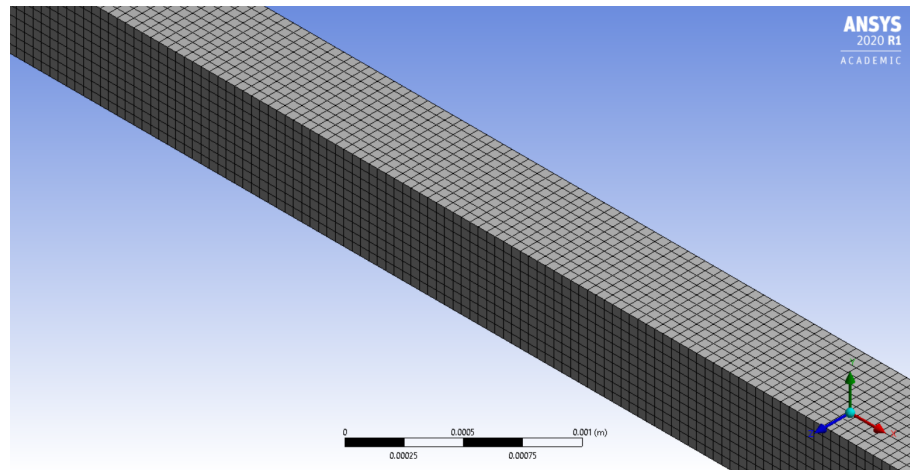


Figure 2.4: Computational mesh for water in a 500 μm channel.

IX71 inverted fluorescent microscope. Fluorescent polymer microspheres 0.52 μm in diameter (0.52 μm , Fluoro-Max red fluorescent polymer microspheres, ThermoScientific, Fermont, CA, USA) were added to the fluid with an approximate volume fraction of 0.3%. The fluid was pumped into the channel from a 1 mL syringe through a length of tubing by a low pressure neMYSYS 290N syringe pump [31] at flow rates ranging from 0.1 to 250 $\mu\text{L/hr}$. The neMYSYS pump is computer controlled and provides accurate pulsation-free flow. To avoid having the height of the pump influence velocity, the pump was set up with two syringes, one to inject fluid and one to withdraw it at the same rate.

The fluorescent particles were illuminated with green light using an X-Cite 120Q light source and imaged in the red. They were visualized using a high-speed camera (Metek Vision Research Phantom VEO 340L) connected to the microscope, at frame rates ranging from 32 to 806 frames per second. A 40 \times objective was used to image all the channels with the exception of the 500 μm channel, for which a 20 \times objective was used.

A time series of images like the one shown in Figure 2.5 was taken with the microscope focused at the bottom of the channel. Using the microscope's focus knob to adjust the position of the focal plane, this was repeated for 8 more evenly spaced planes spanning the channel's height. The images were cross-correlated in LaVision's DaVis software [32] to give a velocity field as seen in Figure 2.6. The velocity data were extracted and plotted using the in-house MATLAB code `pivplot3davg.m` (Appendix A).

Figure 2.5 displays an image of lightly mixed 0.3 wt% Carbopol flowing in a 500 μm channel at a rate of 100 $\mu\text{L/hr}$, as imaged by the PIV system. The bright dots are images of the fluorescent microspheres that were mixed into the fluid. Cross-correlation involves comparing two sequential images and noting how far and in what direction the particles moved between images. From this information the DaVis software calculates the velocity of the particles at each point along the channel and displays it using a colour map. An example velocity field calculated by the software is shown in Figure 2.6.

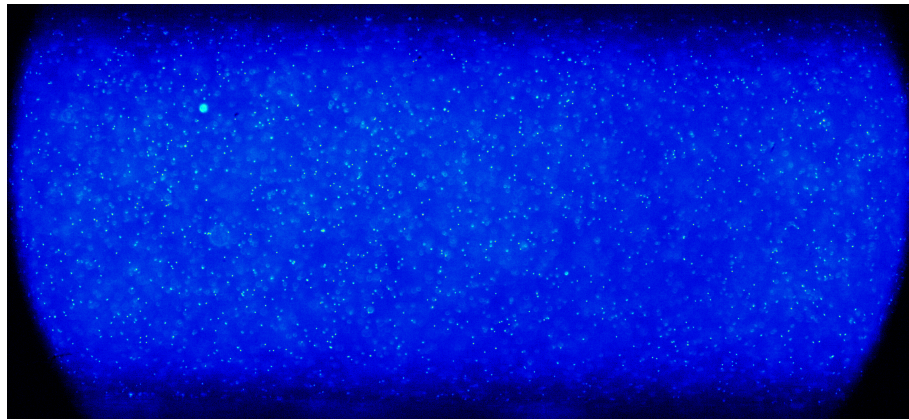


Figure 2.5: An example of a fluorescent particle image from a time series used in the PIV measurements. Lightly mixed 0.3 wt% Carbopol flowing at 100 $\mu\text{L/hr}$ through a 500 μm channel. The bright points are images of the 0.52 μm fluorescent tracer particles suspended in the Carbopol.

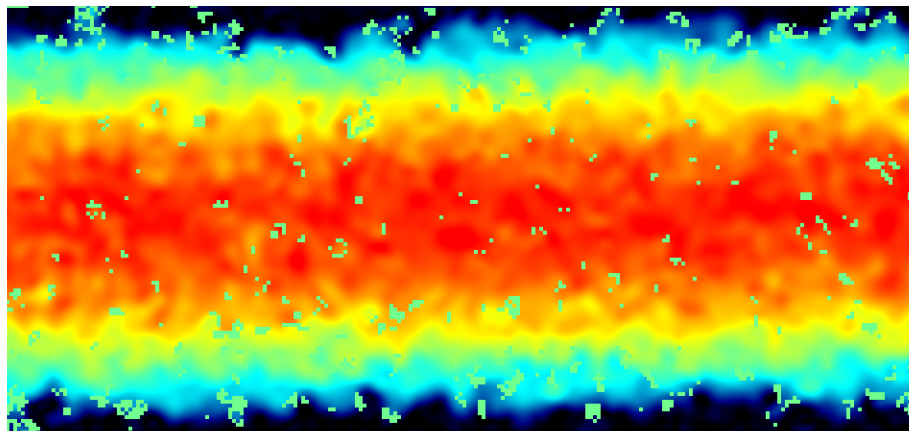


Figure 2.6: Velocity field measured for water flowing through a 500 μm channel at 100 $\mu\text{L/hr}$. The velocity ranges from 0 $\mu\text{m/s}$ (light blue) at the wall to 135 $\mu\text{m/s}$ in the centre (red).

Chapter 3

Results

The size of Carbopol and PNIPAM microgel particles was characterized using dynamic light scattering. Rheological parameters of all experimental fluids were measured. These parameters were also used in simulations of the flow of water in 1 cm long square microchannels ranging in width from 100 μm to 500 μm . The effect of microchannel size on fluid flow behaviour was studied experimentally by injecting the fluids into microchannels that were fabricated using a soft lithography method. The resulting velocity profiles were compared to one another. The profiles of water were compared to the numerical simulations and the profiles of Carbopol and PNIPAM were analyzed using approximate calculations.

3.1 Dynamic Light Scattering

Dynamic light scattering (DLS) was performed using an ALV / CGS-3 compact goniometer with a 22 mW helium-neon laser to measure the average hydrodynamic radius of dissolved particles in dilute Carbopol and PNIPAM solutions at an angle of 30° . PNIPAM and pH 6 Carbopol were diluted with deionized water to ensure that the dynamic light scattering measurements were not influenced by multiple scattering of light.

3.1.1 Carbopol

The output of the ALV system is the intensity autocorrelation function of the scattered light as a function of correlator delay time. Figure 3.1 shows the correlation functions obtained for lightly and vigorously mixed 2.80×10^{-2} wt% Carbopol at 20°C. At long times, the data were strongly influenced by slow drifts in electronics and the environment. At short times, the data were noisy. For this reason, the data at high and low times were discarded. The red points represent the data used to determine the particle size and the blue points represent the data that were discarded. If the scattering particles were monodisperse, the correlation function would decay exponentially, with the decay time being related to the mobility, and thus the size, of the particles. In reality the decay is non-exponential and represents a convolution of the decays due to a distribution of particle sizes.

The correlation function describes how much scattered light is being detected over time. The larger the particle, the slower it moves and there are slower fluctuations in the scattered light. When a particle is small it moves quickly and the fluctuations in the detected intensity are rapid. Where the correlation function drops off indicates the exponential decay time. The exponential decay time is the time associated with the most common particle size.

Using a regularized inverse Laplace transform method, the correlation function was used to determine the particle radius distribution function. The distribution function was normalized so that it peaks at a value of one. Examples of the distribution function calculated for Carbopol are shown in Figure 3.2. The first moment of the distribution gives the mean hydrodynamic radius of the particles. The square root of the second moment gives the standard deviation. The standard deviation is a measure of the polydispersity of the particles.

Using the first and second moments of Figure 3.2, the hydrodynamic radius was found to be $19 \pm 16 \mu\text{m}$ for lightly mixed Carbopol and $4 \pm 1 \mu\text{m}$ for vigorously mixed Carbopol. Vigorously

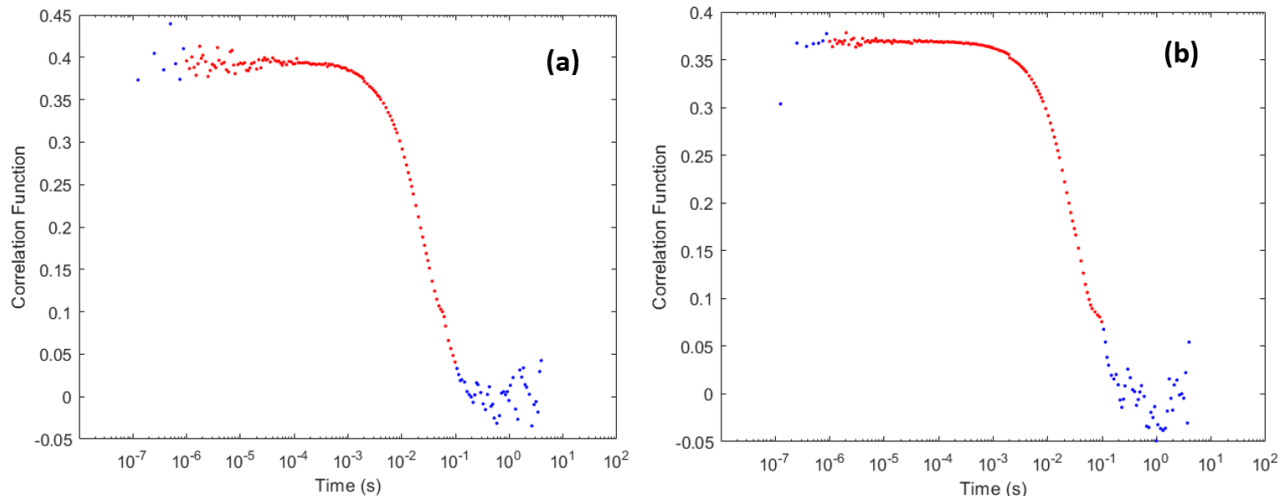


Figure 3.1: Autocorrelation function of the scattered light intensity for 2.80×10^{-2} wt% (a) lightly mixed and (b) vigorously mixed Carbopol solution at 20°C and an angle of 30° . The correlation function was measured using dynamic light scattering and is shown as a function of delay time. The blue points indicate data that were discarded and the red points indicate the data included in the determination of the particle size distribution.

lightly mixed Carbopol displayed a second peak at a much larger particle size. This second peak could be due to dust or a cluster of particles, or long-term drifts in the electronics. Because scattering intensity increases with particle radius r roughly as r^6 , this peak represents a very small number of large scatterers and so can be ignored. Comparing lightly and vigorously mixed Carbopol shows that mixing time had a significant impact on the size and polydispersity of Carbopol 940 particles. Particles of vigorously mixed Carbopol are both smaller and less polydisperse than particles of lightly mixed Carbopol.

Using dynamic light scattering measurements on a different type of Carbopol (Ultrez U10), Dinkgreve, et al. also found a significant size difference when mixing time was increased. They found a lightly mixed sample to have a particle size of approximately $10 \mu\text{m}$ and a vigorously mixed sample to have a particle size of approximately $1 \mu\text{m}$ [23]. Dinkgreve, et al. also used confocal microscopy to observe smaller and less polydisperse particles in the vigorously mixed sample [23]. Using confocal microscopy, Lee et al. found that stirring Carbopol (ETD

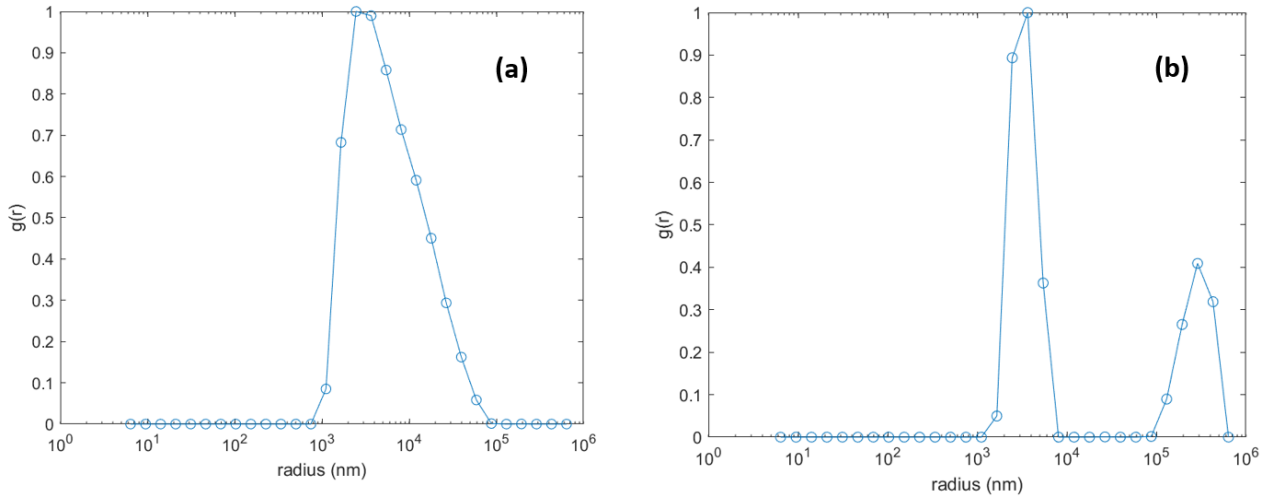


Figure 3.2: Particle radius distribution function of (a) lightly mixed and (b) vigorously mixed Carbopol solution. The width of the distribution function spans the size of the microgel particles and reflects polydispersity.

2050) for 24 hours gave a particle size of approximately $3 \mu\text{m}$ while an unstirred Carbopol solution had an approximate particle size of $6 \mu\text{m}$ [12].

3.1.2 PNIPAM

Three samples of PNIPAM were prepared using the compositions in Table 2.1. Using the same DLS method as Carbopol, the particle size distribution function of 5×10^{-3} wt% Medium BIS and 6.24×10^{-3} wt% High BIS PNIPAM were measured over a temperature range of 15°C to 40°C . The temperature of the diluted PNIPAM was initially set to 20°C and data were collected as the sample was heated in steps to higher temperatures with a wait time of at least 10 minutes. The sample was then cooled back down to 20°C then further cooled to collect data at lower temperatures.

The correlation functions of Medium BIS PNIPAM at 15 , 20 , 35 , and 40°C are shown in Figure 3.3. As above, data at high and low delay times were discarded.

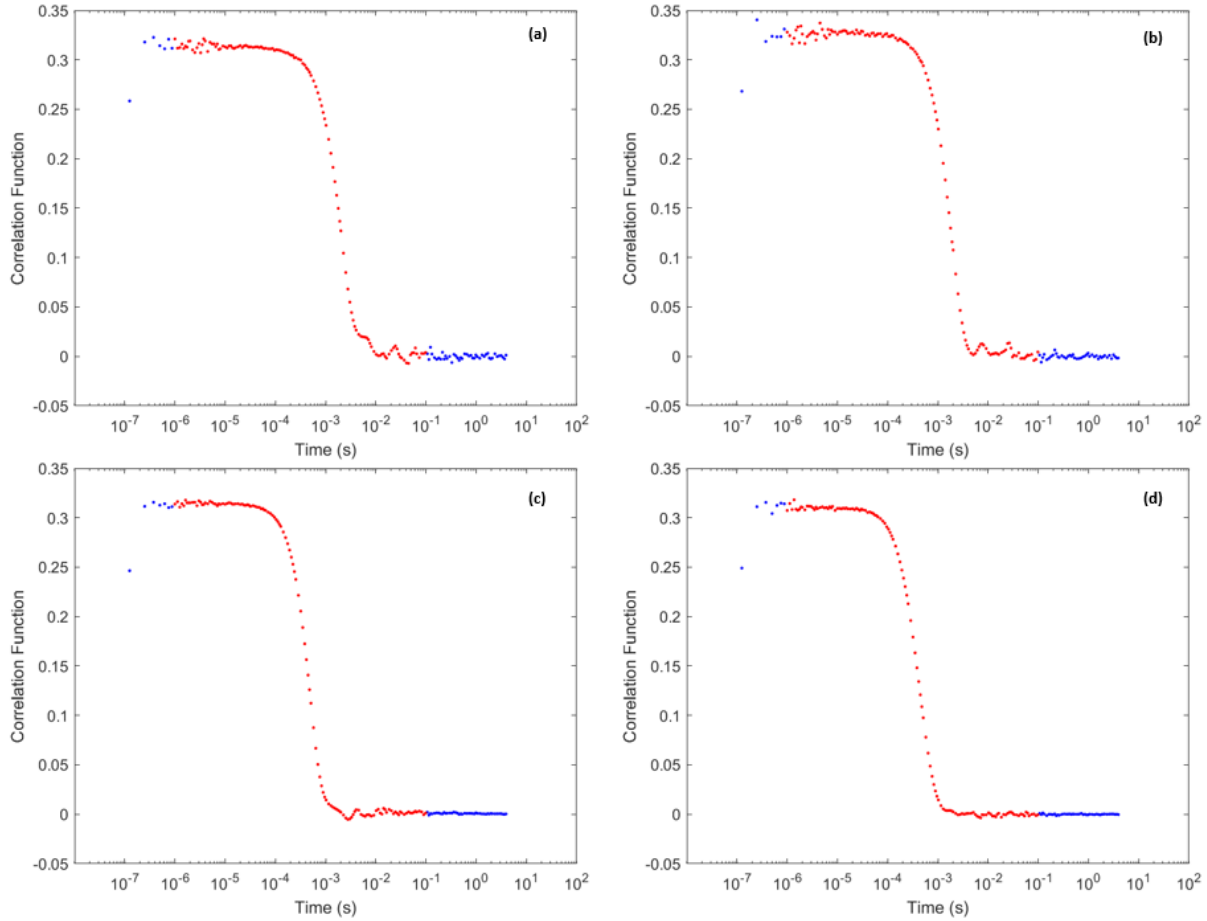


Figure 3.3: Autocorrelation function of the scattered light intensity for 10 wt% Medium BIS PNIPAM at (a) 15°C, (b) 20°C, (c) 35°C, and (d) 40°C. The correlation function was measured using dynamic light scattering and is shown as a function of delay time. The blue points indicate data that were discarded and the red points indicate the data included in the determination of the particle size distribution.

Using a regularized inverse Laplace transform method, the correlation function was used to calculate the particle radius distribution function, Figure 3.4. The first and second moments of the distribution function were used as the hydrodynamic radius and its standard deviation, respectively. The hydrodynamic radius is plotted as a function of temperature in Figure 3.5 and the standard deviation is shown using error bars.

As Figure 3.5 shows, the radius of the PNIPAM particles decreased monotonically as temper-

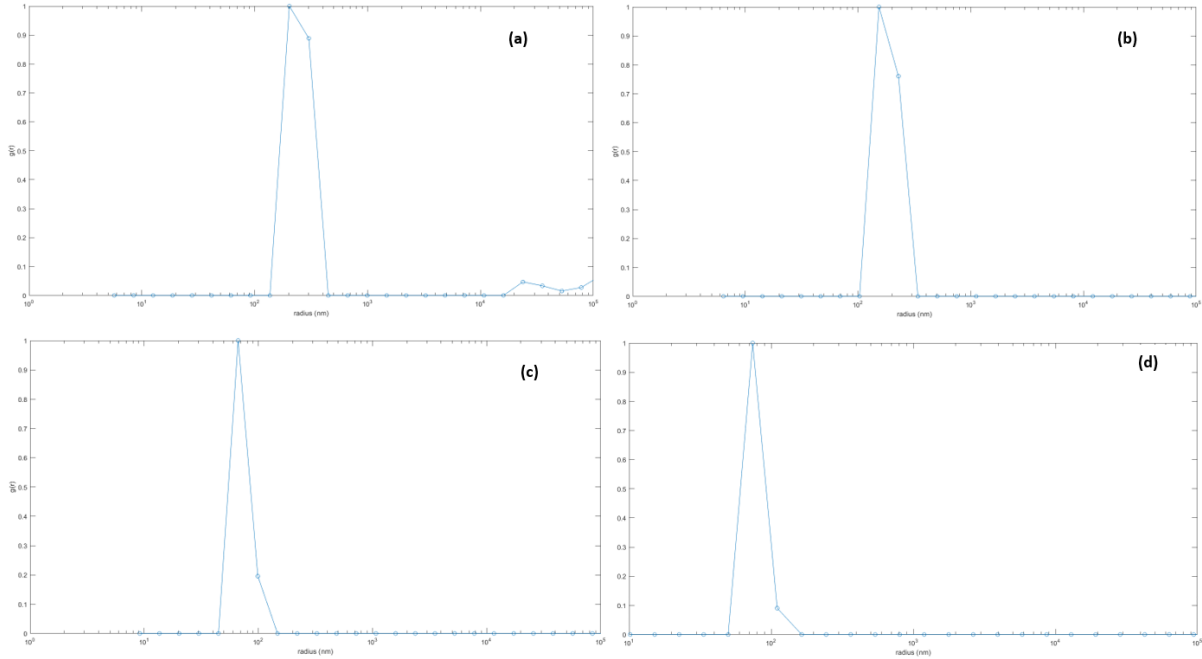


Figure 3.4: Particle radius distribution function of 10 wt% Medium BIS PNIPAM at (a) 15°C, (b) 20°C, (c) 35°C, and (d) 40°C. The width of the distribution function gives the size of the solution's particles and its polydispersity.

ature increased, experiencing a significant drop between 25 and 35°C. The error bars indicate the polydispersity of PNIPAM, which has no systematic dependence on temperature. There was, however, a dependence on BIS concentration. Medium BIS PNIPAM has a BIS concentration of 1.87 wt% and High BIS PNIPAM a concentration of 6.74 wt%. At 20°C, the same temperature used for the Carbopol measurements, Medium BIS PNIPAM has a particle size of 190 ± 40 nm and High BIS PNIPAM a particle size of 140 ± 20 nm, indicating that the greater the BIS concentration the smaller the mean particle size is. Medium BIS PNIPAM consistently has a larger particle size than High BIS PNIPAM across the temperature range, however the size ratio is not consistent. The mean particle size of both PNIPAM samples is significantly smaller than the mean particle size of Carbopol.

Our PNIPAM was prepared by closely following the polymerization method laid out by Senff and Richtering in [16]. Senff and Richtering also performed DLS experiments on PNIPAM

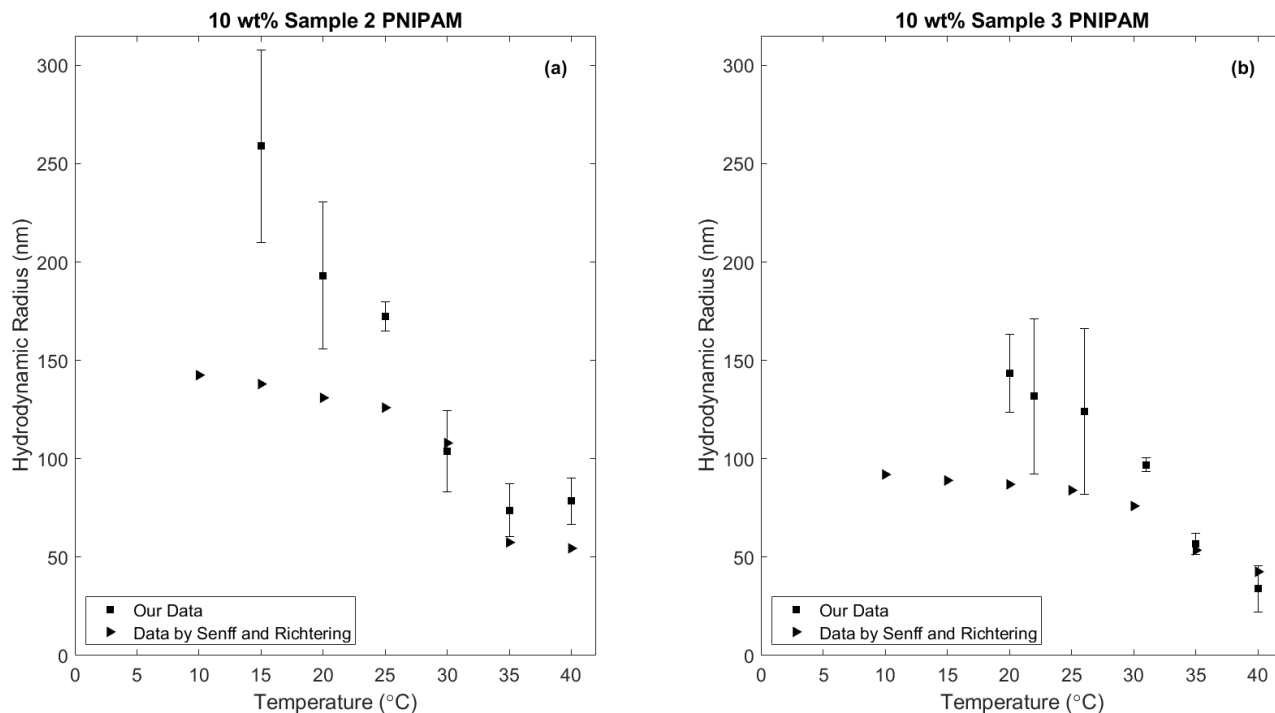


Figure 3.5: Mean radii of dissolved (a) Medium BIS and (b) High BIS PNIPAM particles measured by dynamic light scattering according to our measurements and measurements by Senff and Richtering [16], plotted as a function of temperature. The error bars represent the standard deviation.

using an ALV goniometer. Their results for the hydrodynamic radius, extracted from [16], are also plotted in Figure 3.5. They also found that the hydrodynamic radius decreased as temperature increased, with a significant drop occurring between 25 and 35°C. Senff and Richtering found the same dependence of BIS concentration on particle size, increasing the BIS concentration results in a decrease in mean particle size.

The temperature range at which we see a significant drop in the hydrodynamic radius is consistent with the value of the LCST, 31 - 34°C, measured by [16–19]. Although we followed the same synthesis procedure for PNIPAM, there is a significant difference between our values of the hydrodynamic radius measured and those measured by Senff and Richtering [16]. Our values, for both samples, are, on average, a factor of 1.4 larger than those measured by Senff and Richtering. This discrepancy could be a result of differences in sample preparation, or may

indicate that our solutions were not dilute enough and that our data are affected by multiple scattering.

3.2 Rheology

3.2.1 Carbopol

Flow Curves

The flow curves of Carbopol and PNIPAM were measured using an Anton Paar MCR302 shear rheometer with a 4° cone-and-plate tool. 600 grit sandpaper was affixed to both the rheometer tool and the bottom plate. The temperature was set to 20°C for Carbopol, while the temperature was varied from 5°C to 40°C for PNIPAM. The shear rate was increased in steps from 0.01 s⁻¹ to 100 s⁻¹ and then immediately decreased in steps to 0.01 s⁻¹ to test for hysteresis. The resulting shear stress was measured with a wait time varying from 180 s at low shear rates down to 10 s at high shear rates.

The data was fit to the Herschel-Bulkley model, $\sigma = \sigma_y + k\dot{\gamma}^n$, to give the yield stress, σ_y , consistency index, k , and flow index, n . The uncertainties given below are the standard deviations in the parameters as determined by the fitting routine.

The flow curves for Carbopol are shown in Figure 3.6 along with the fits. The fit parameters are given in Table 3.1. The fits show that yield stress increases with concentration, as expected. The fits also show that the yield stress of the vigorously mixed samples is significantly larger than the yield stress of the lightly mixed samples of the same concentration. Dinkgreve, et al. measured flow curves for 0.6 wt% Carbopol Ultrez U10, a different kind of Carbopol, for stirring times of 2 hours, 10 hours, and 20 hours at 2000 rpm. In contrast to our results, they showed that increasing stirring time decreases the yield stress [23]. This discrepancy is un-

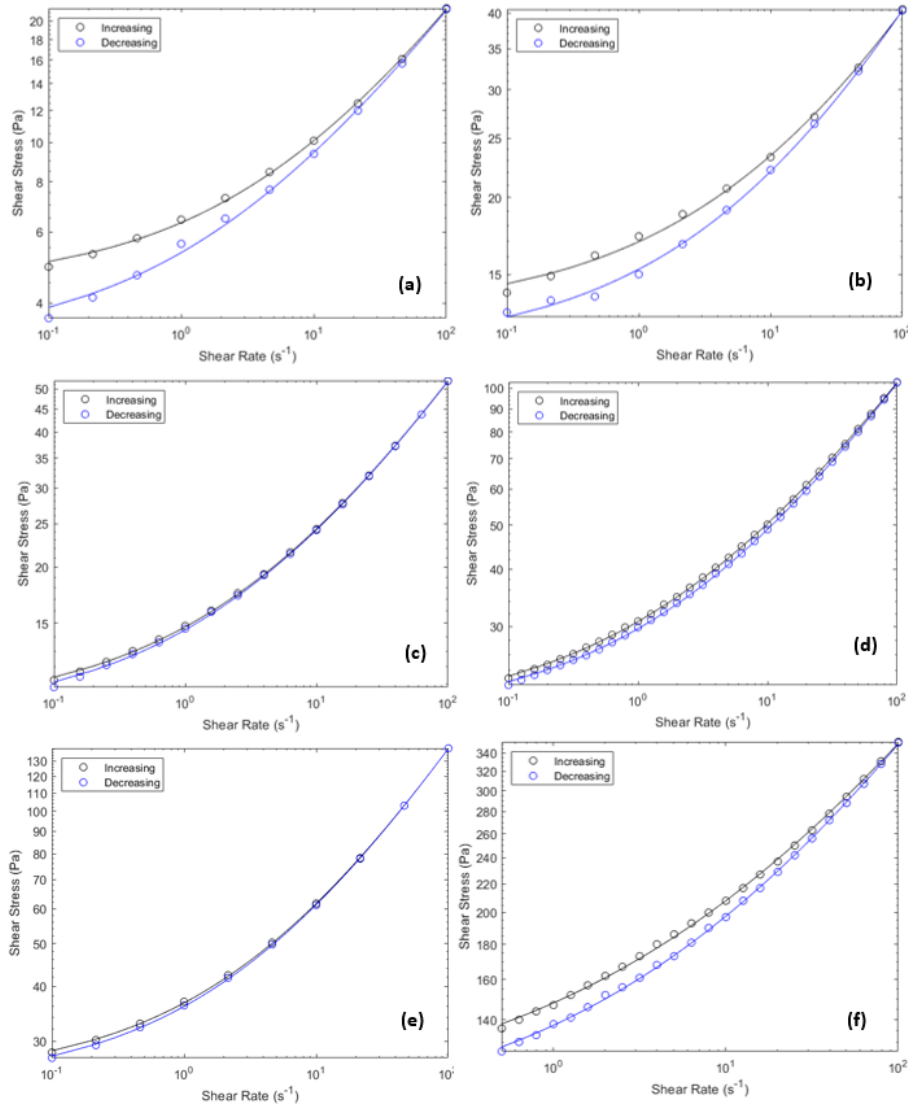


Figure 3.6: Shear stress vs. shear rate of Carbopol samples fitted to the Herschel-Bulkley model. The circles represent the data measured and the lines are the Herschel-Bulkley fit. a) lightly mixed 0.14 wt% Carbopol, b) vigorously mixed 0.14 wt% Carbopol, c) lightly mixed 0.3 wt% Carbopol, d) vigorously mixed 0.3 wt% Carbopol, e) lightly mixed 1 wt% Carbopol, f) vigorously mixed 1 wt% Carbopol.

Table 3.1: Fit parameters determined by fitting the flow curve of Carbopol samples to the Herschel-Bulkley model, $\sigma = \sigma_y + k\dot{\gamma}^n$. Measurements were done with shear rate increasing from low to high and decreasing from high to low. Uncertainties are the standard deviations determined by the fitting routine. “Light” refers to samples that were mixed for 1 hour after NaOH was added and “vigorous” refers to samples that were mixed for 24 hours after NaOH was added.

Sample	Yield Stress, σ_y (Pa)	Consistency Index, k (Pa · s ⁿ)	Flow Index, n
Increasing			
0.14 wt% Carbopol, light	4.4 ± 0.1	1.9 ± 0.1	0.48 ± 0.01
0.14 wt% Carbopol, vigorous	12.9 ± 0.4	4.0 ± 0.4	0.42 ± 0.02
0.3 wt% Carbopol, light	9.57 ± 0.08	5.15 ± 0.07	0.458 ± 0.003
0.3 wt% Carbopol, vigorous	18.8 ± 0.1	11.90 ± 0.09	0.424 ± 0.002
1 wt% Carbopol, light	24.6 ± 0.2	12.1 ± 0.2	0.488 ± 0.003
1 wt% Carbopol, vigorous	104 ± 2	43 ± 2	0.377 ± 0.007
Decreasing			
0.14 wt% Carbopol, light	3.1 ± 0.2	2.2 ± 0.2	0.46 ± 0.02
0.14 wt% Carbopol, vigorous	11.3 ± 0.3	4.0 ± 0.3	0.43 ± 0.01
0.3 wt% Carbopol, light	9.2 ± 0.1	5.3 ± 0.1	0.454 ± 0.004
0.3 wt% Carbopol, vigorous	18.7 ± 0.1	10.9 ± 0.1	0.442 ± 0.002
1 wt% Carbopol, light	23.8 ± 0.2	12.3 ± 0.2	0.486 ± 0.003
1 wt% Carbopol, vigorous	98 ± 1	39 ± 1	0.404 ± 0.005

expected, but may relate to differences in sample preparation or the difference in the type of Carbopol.

As seen in Figure 3.6 and Table 3.1, the rheological parameters measured for increasing and decreasing strain rate are significantly different for the 0.14 wt% samples and vigorously mixed 1 wt%. Although Carbopol is widely regarded as a simple yield-stress fluid with no hysteresis [33–40], there have been studies that show that Carbopol does not always behave as a simple yield-stress fluid and can display hysteresis [41].

Hysteresis is an indication of thixotropy. A fluid is considered thixotropic when its viscosity is time dependent. The increasing flow curve was always measured first. As the applied shear rate increased the viscosity of the fluid decreased. The decreasing flow curve was measured immediately following the increasing. Since the viscosity took time to recover, the decreasing flow curve was always less than the increasing curve.

Amplitude Sweeps

The storage and loss moduli of Carbopol were measured as a function of frequency under small-amplitude oscillatory shear. To determine the extent of the linear viscoelastic regime of Carbopol, a constant frequency of 1 s^{-1} was applied as the amplitude of the oscillating strain was increased from .01% to 1000%.

Results from the amplitude sweeps, shown in Figure 3.7, are consistent with what is expected. Each graph in the figure can be divided into 3 regions: the linear viscoelastic regime, the yielding regime, and the non-linear regime. The linear viscoelastic regime occurs at low strain amplitudes and is characterized by constant values of the viscous and elastic moduli. Here the strain being applied is small in comparison to the strain needed to disrupt the interactions between Carbopol particles. In this regime, the storage modulus is greater than the loss modulus,

indicating that Carbopol displays a primarily elastic behaviour at low strain amplitudes. The yielding region is located around the crossover point. Here the structure of the sample begins to break down. The nonlinear region begins after the crossover point. Here the storage modulus is decreasing much faster than the loss modulus and material is more viscous than elastic [10]. These results are consistent with other rheological characterizations of Carbopol [10, 11].

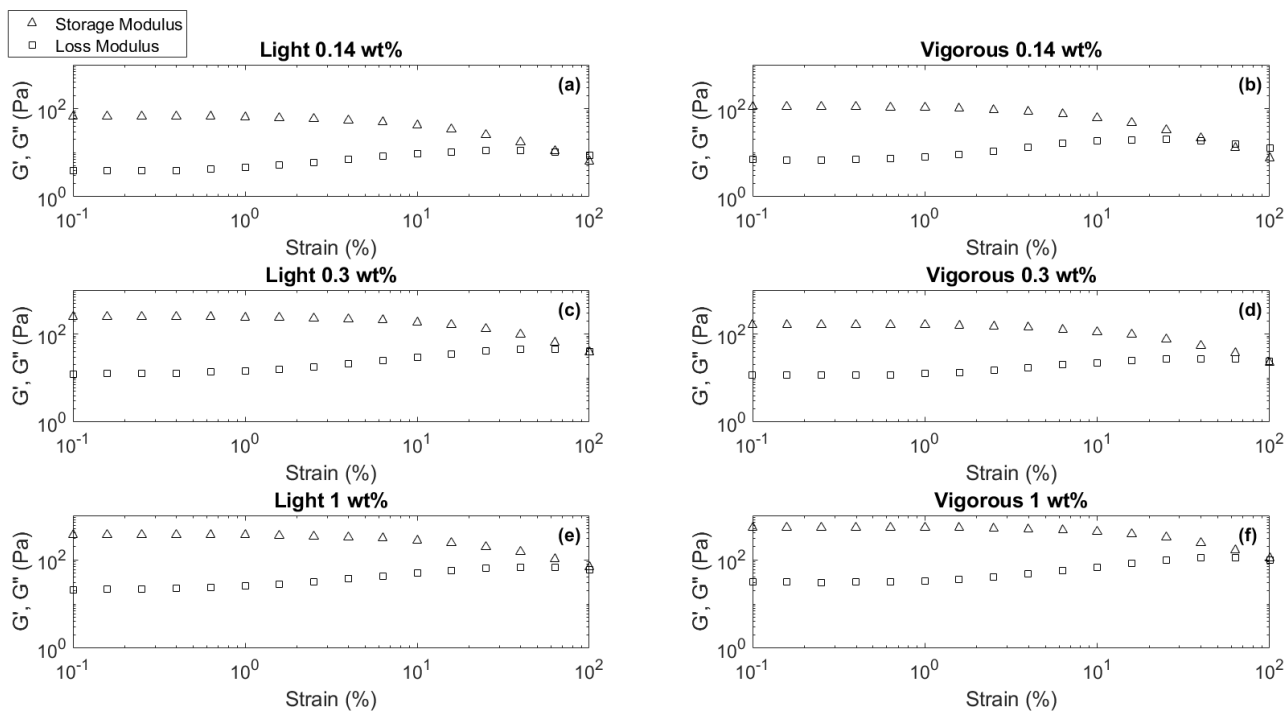


Figure 3.7: The storage (G') and loss modulus (G'') of Carbopol as a function of the amplitude of the applied oscillatory strain. a) Lightly mixed 0.14 wt% Carbopol, b) Vigorously mixed 0.14 wt% Carbopol, c) Lightly mixed 0.3 wt% Carbopol, d) Vigorously mixed 0.3 wt% Carbopol, e) Lightly mixed 1 wt% Carbopol, f) Vigorously mixed 1 wt% Carbopol.

Frequency Sweeps

A frequency sweep was used to measure the storage and loss modulus as angular frequency was increased from 0.01 to 1000 s^{-1} at a constant strain rate that was within the linear viscoelastic regime. A strain of 1% was used for lightly mixed Carbopol samples and a strain of 0.2% was used for vigorously mixed Carbopol samples. The frequency sweeps, Figure 3.8, reveal that the storage modulus remains essentially constant and larger than the loss modulus for the bulk of the frequency range, which is what is expected for crosslinked macromolecules like Carbopol [42, 43] and is consistent with other rheological characterizations of Carbopol [10, 11].

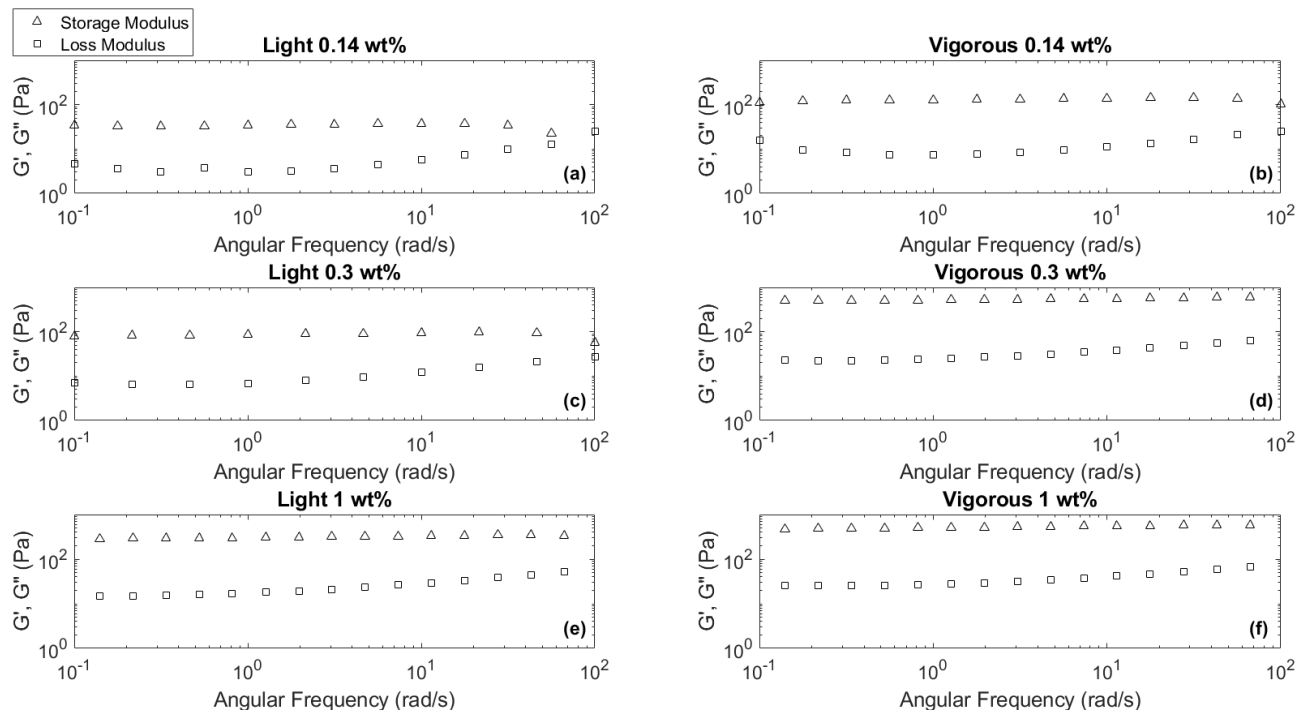


Figure 3.8: The storage (G') and loss modulus (G'') of Carbopol as a function of angular frequency. a) lightly mixed 0.14 wt% Carbopol, b) vigorously mixed 0.14 wt% Carbopol, c) lightly mixed 0.3 wt% Carbopol, d) vigorously mixed 0.3 wt% Carbopol, e) lightly mixed 1 wt% Carbopol, f) vigorously mixed 1 wt% Carbopol.

Creep Tests

In a creep test, a constant shear stress is applied to a previously unstrained fluid and the time evolution of strain is recorded. Here, the desired stress was applied to the Carbopol samples for 333 s followed by a constant stress of 0 Pa for another 333 s. The resulting strain was measured over time. Figure 3.9 shows the results of creep tests for the Carbopol samples. Initially the strain increases at a rapid rate. As the applied stress is increased beyond the yield stress, a creep test reveals an increasingly more linear behaviour. Recovery from the stress begins once the applied stress is removed. Here stored elastic stresses relax and the elastic deformation of the sample is able to recover fully. The yield stress lies between the highest applied stress that gives a profile with a constant strain and the lowest applied stress that gives a profile with a linear behaviour. The range where the yield stress lies is given in Table 3.2.

Table 3.2: Yield stresses obtained from flow curves and creep tests. The values from the flow curves were obtained by fitting the data to the Herschel-Bulkley model. The uncertainties are the standard deviations. The yield stresses from the creep tests are given as a range indicating the stress between the highest applied stress that gives a profile with a constant strain and the lowest applied stress that gives a profile with a linear behaviour.

Test		0.14 wt% (Pa)	0.3 wt% (Pa)	1 wt% (Pa)
Light	Creep Test	4-5		20-30
	Increasing Flow Curve	4.4 ± 0.1	9.57 ± 0.08	24.6 ± 0.2
	Decreasing Flow Curve	3.13 ± 0.2	9.2 ± 0.1	23.8 ± 0.1
Vigorous	Creep Test	12-13	17-18	100-110
	Increasing Flow Curve	12.9 ± 0.4	18.8 ± 0.1	104 ± 2
	Decreasing Flow Curve	11.3 ± 0.3	18.7 ± 0.1	98 ± 1

A creep test gives what is referred to as the static yield stress. The yield stress obtained from fitting the Herschel-Bulkley model to a flow curve is referred to as the dynamic yield stress. Generally, these two yield stresses are distinct from one another, with the dynamic yield stress being smaller than the static yield stress [44]. The values of the dynamic yield stress obtained from increasing and decreasing flow curves are within or close to the range found for the static yield stress range.

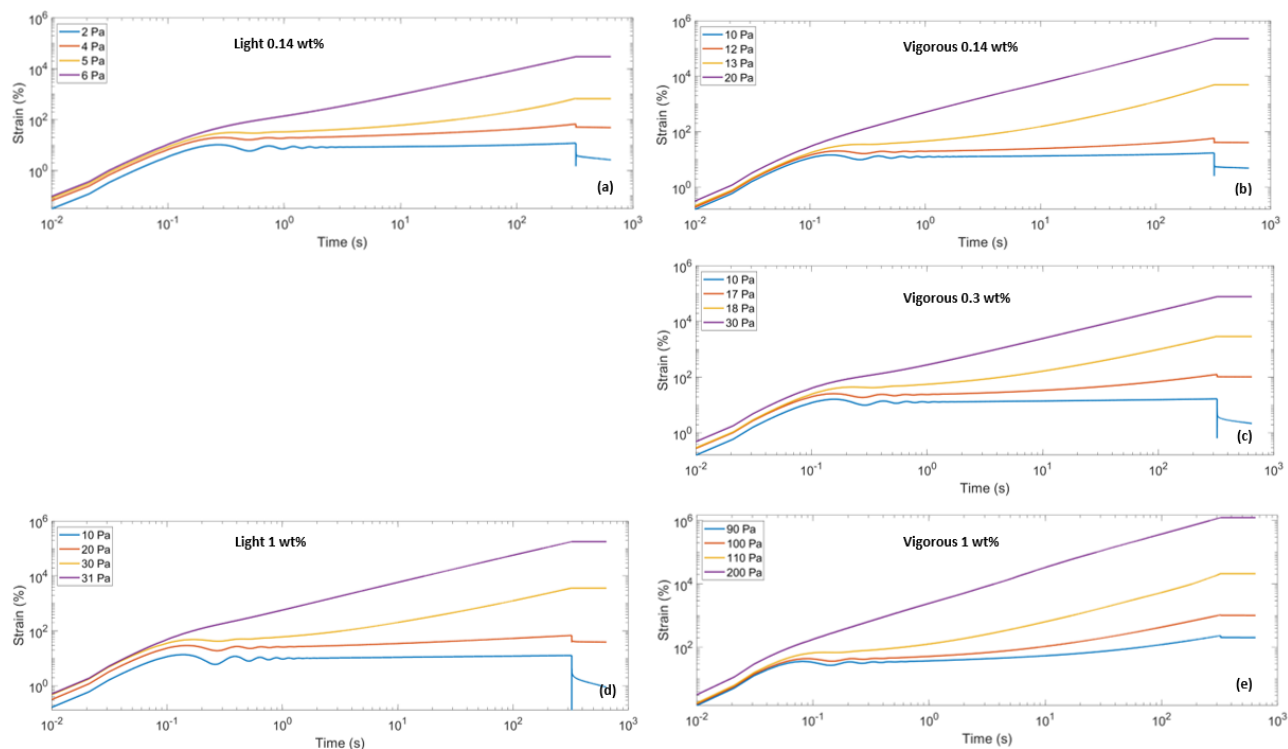


Figure 3.9: Creep tests of a) lightly mixed 0.14 wt% Carbopol, b) vigorously mixed 0.14 wt% Carbopol, c) vigorously mixed 0.3 wt% Carbopol, d) lightly mixed 1 wt% Carbopol, e) vigorously mixed 1 wt% Carbopol. The labelled shear stress was applied for 333 s followed by 0 Pa being applied for 333 s. The yield stress of each sample lies between the highest applied stress that gives a profile with a constant strain and the lowest applied stress that gives a profile with a linear behaviour.

3.2.2 PNIPAM

Flow Curves

Three samples of PNIPAM were prepared using the compositions in Table 2.1. Flow curves of 10 wt% PNIPAM were measured for a temperature range of 5 to 40°C. Data for selected temperatures are plotted in Figure 3.10. Often the flow curves show the decreasing curve lying slightly above the increasing one, suggesting that some evaporation occurred during the test. At 40 °C the PNIPAM sample was well above its LCST and could no longer be fit to the Herschel-Bulkley model. The Herschel-Bulkley parameters obtained from fits to the data at these and other temperatures are plotted as functions of temperature in Figure 3.11.

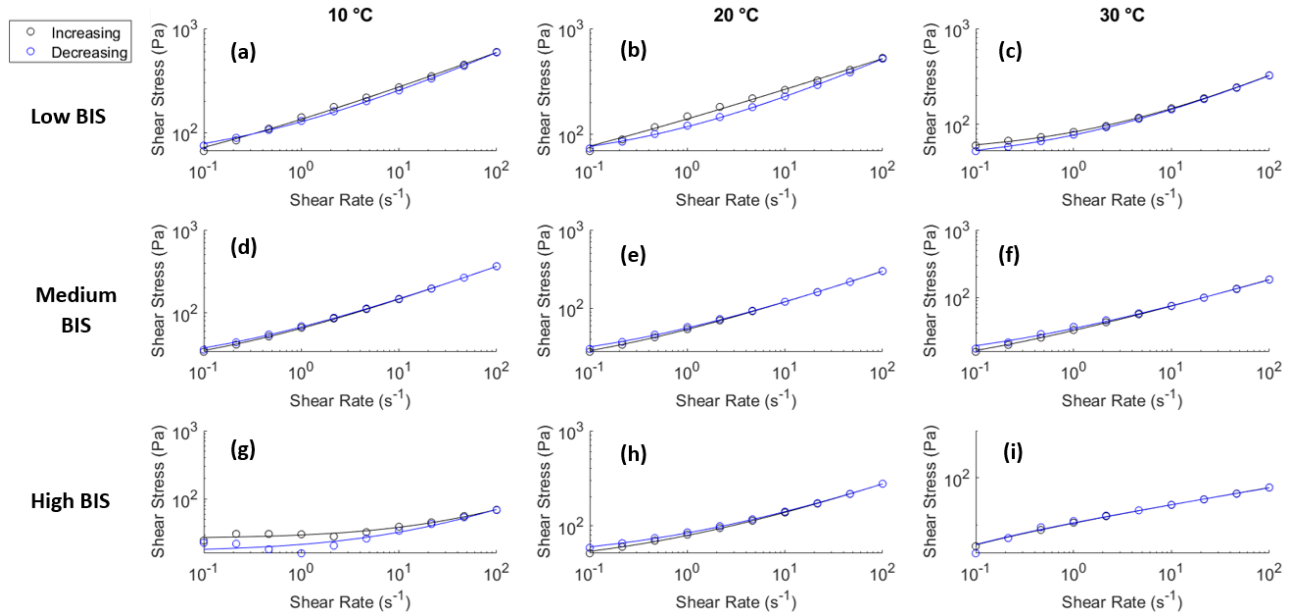


Figure 3.10: Shear stress vs. shear rate of 10 wt% PNIPAM, with 3 different BIS concentrations, for 10, 20, and 30°C fitted to the Herschel-Bulkley model. Measurements were done with shear rate increasing from 0.01 s⁻¹ to 100 s⁻¹ in steps and decreasing from 100 s⁻¹ to 0.01 s⁻¹ in steps. The circles represent the data measured and the lines are the Herschel-Bulkley fit.

Low BIS PNIPAM flow curves did not have much curvature making it hard to fit to the Herschel-Bulkley model. This resulted in relatively large uncertainties in the parameters and likely contributed to the significant difference between parameters for increasing and decreasing flow curves shown in Figure 3.11. Medium BIS and High BIS PNIPAM show a decrease in yield stress and consistency index as temperature increases, while the power law index remains relatively constant. At 10°C, High BIS PNIPAM displays a lower yield stress than at 15°C. This is unexpected and worth revisiting.

Temperature Sweeps

At a constant shear rate of 50 s⁻¹, the temperature of 10 wt% PNIPAM, with 3 different BIS concentrations, was increased constantly from 5°C to 40°C at a rate of 0.25°C per minute for each sample. The resulting stress is related to viscosity by Newton's law of viscosity, $\sigma = \eta\dot{\gamma}$.

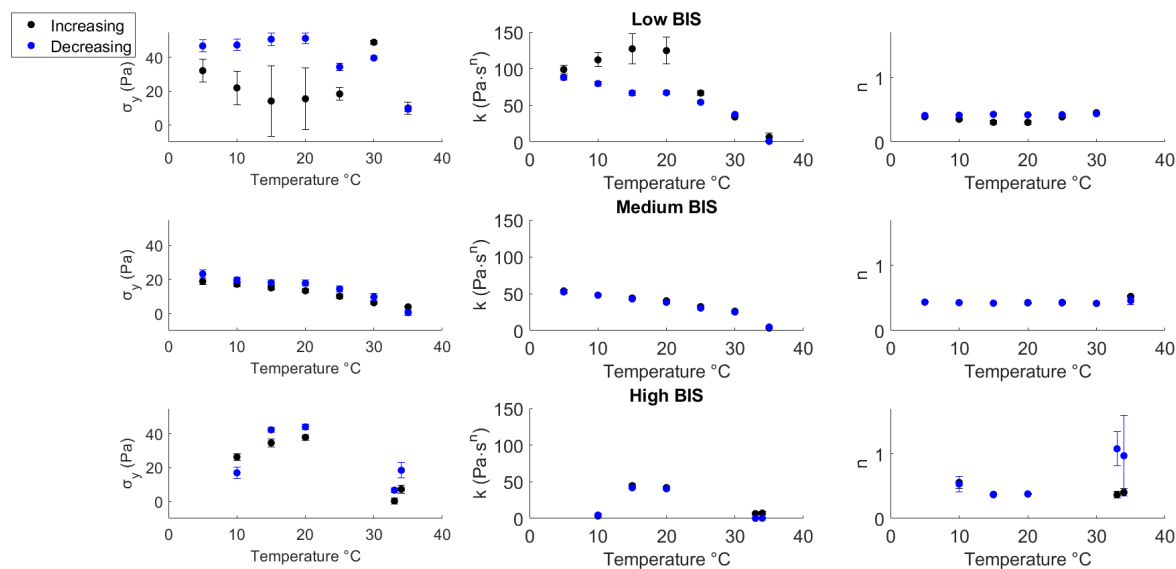


Figure 3.11: Herschel-Bulkley parameters for 10 wt% PNIPAM, with 3 different BIS concentrations, for increasing and decreasing flow curves at temperatures ranging 5 to 35°C. First row shows Low BIS, the middle row Medium BIS, and the last row High BIS. a) Low BIS yield stress, b) Low BIS consistency index, c) Low BIS power law index, d) Medium BIS yield stress, e) Medium BIS consistency index, f) Medium BIS power law index, g) High BIS yield stress, h) High BIS consistency index, i) High BIS power law index.

Low BIS PNIPAM displayed the highest viscosity at low temperatures and High BIS PNIPAM displayed the lowest viscosity. As displayed in Figure 3.12, the viscosity of 10 wt% PNIPAM decreases approximately linearly with temperature until around 25°C, where there is a change in slope and a nonlinear temperature dependence. Above 33°C, the LCST, the viscosity approaches a constant value.

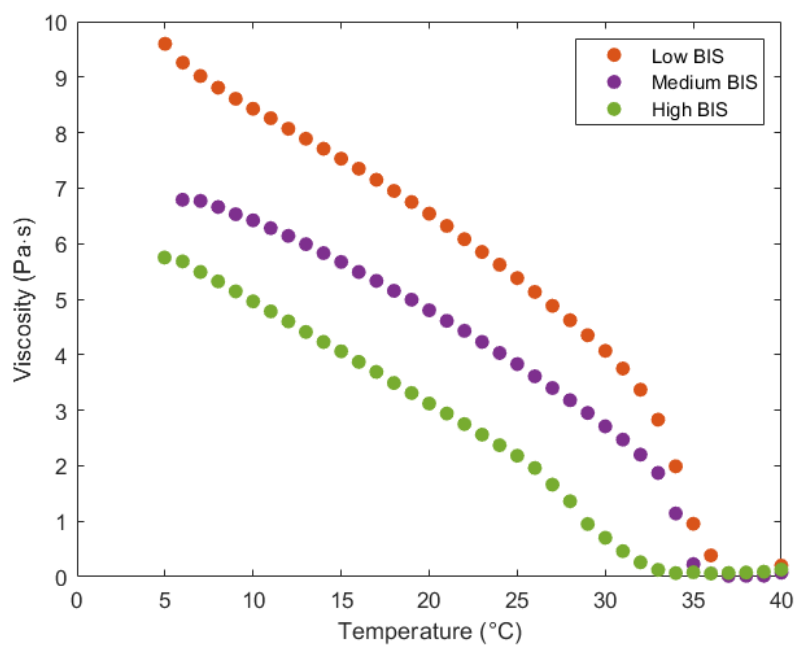


Figure 3.12: Viscosity of 10 wt% PNIPAM, with 3 different BIS concentrations, at a constant shear rate of 50 s^{-1} as a function of temperature.

3.3 Numerical Modeling

Ansys Fluent software was used to simulate the velocity profiles of water in 1 cm long square microchannels ranging in width from 100 μm to 500 μm . Flow rates ranging 0.1 $\mu\text{L/hr}$ to 250 $\mu\text{L/hr}$ were used in each channel. The velocity across the channel width was taken at half the height, known as the mid-plane, and half the length of the channel.

Figure 3.13 shows the results of water flowing in a 500 μm channel at selected flow rates. Similar profiles were determined for each flow rate and channel studied. The maximum velocity of each profile is shown in Table 3.3. The maximum velocity increased with channel size and with flow rate as expected for a Newtonian fluid.

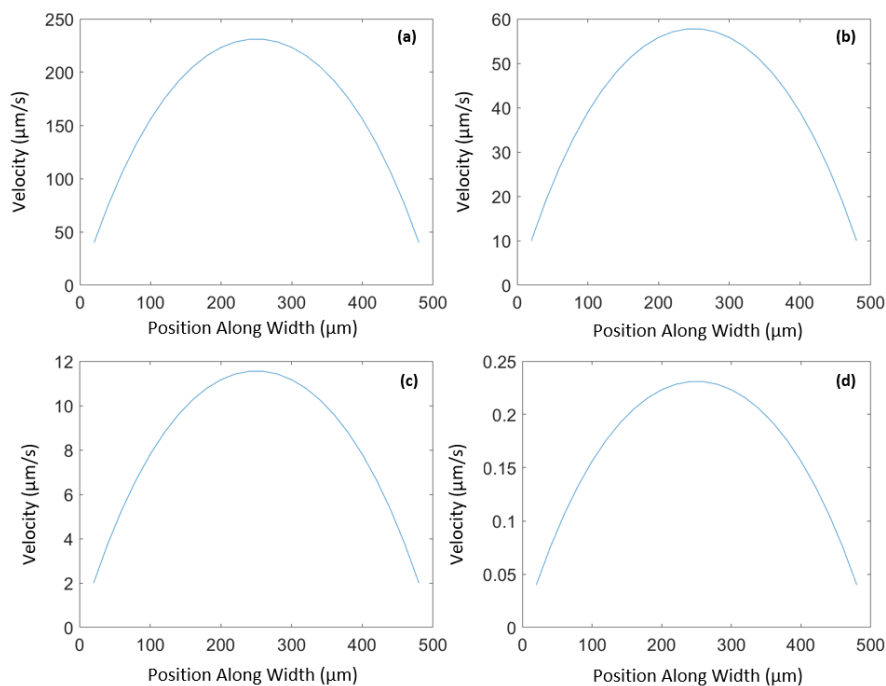


Figure 3.13: Results of Ansys Fluent simulations for water in a 500 μm square channel with a flow rate of (a) 100, (b) 25, (c) 5, and (d) 0.1 $\mu\text{L/hr}$. Flow is displayed for the mid-plane, half way along the 1 cm channel.

3.4 Micro-Particle Image Velocimetry

The fluid samples with 0.52 μm fluorescent microspheres added were injected into the microchannels at flow rates ranging from 0.1 $\mu\text{L/hr}$ to 250 $\mu\text{L/hr}$. Images were collected at nine evenly spaced planes spanning the height of each channel. The images for each plane were cross-correlated using LaVision's DaVis software to give the velocity as a function of position in each plane. A MATLAB code was developed to export and plot the data. The code produced velocity profiles like those shown in Figure 3.14. This figure illustrates the shape of the flow profiles observed for each fluid. Water shows an approximately parabolic profile, while the yield-stress fluids, Carbopol and PNIPAM, display a plug in the centre of the channel.

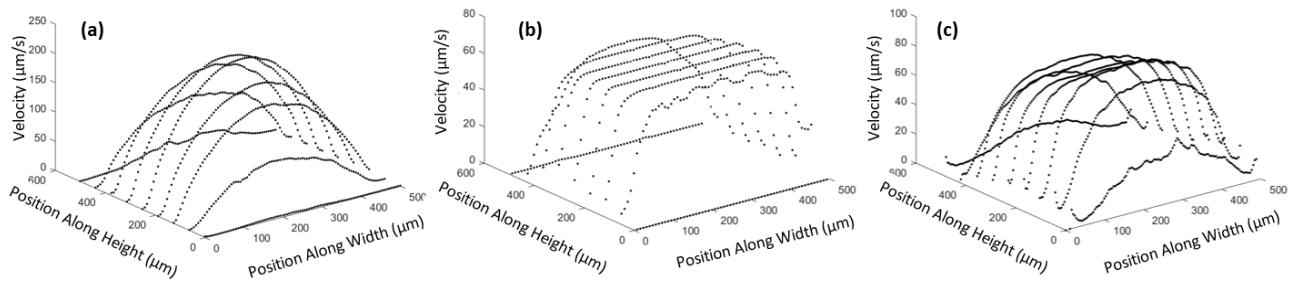


Figure 3.14: Velocity profile of a) water, b) vigorously mixed 0.3 wt% Carbopol, and c) 10 wt% High BIS PNIPAM in a 500 μm square channel at a flow rate of 50 $\mu\text{L/hr}$.

Using another MATLAB code, the maximum of the velocity profile for water in the channel's midplane was determined by fitting a parabola to the curve. For a given channel, the maximum velocity was found to increase as flow rate increased while for a given flow rate, the maximum velocity increased as channel size decreased, as shown in Table 3.3. Since the mean flow velocity is given by $v_{avg} = \frac{Q}{A}$, where v_{avg} is the average velocity, Q is flow rate, and A is the cross-sectional area of the channel this behaviour is in agreement with expectations. Generally, the experimental values agreed, within uncertainty, with that predicted by simulations in Ansys Fluent, bearing in mind that the actual values of the channel dimensions may be different than the nominal values. Table 3.3 shows that slightly higher v_{max} were consistently seen with μPIV compared to the simulations, suggesting the actual channel dimensions were smaller than the

nominal.

Table 3.3: Maximum velocities of water in the mid-plane approximately half way along the 1 cm long channel.

Flow Rate ($\mu\text{L/hr}$)	500 μm v_{max} ($\mu\text{m/s}$)	300 μm v_{max} ($\mu\text{m/s}$)	200 μm v_{max} ($\mu\text{m/s}$)	100 μm v_{max} ($\mu\text{m/s}$)
Ansys Fluent				
250	577	1600	3600	14200
100	231	641	1440	5670
50	115	320	720	2830
25	57.7	160	360	1420
10	23.1	64.1	144	567.0
5	11.5	32.0	72.0	283.0
μPIV				
250	580 ± 20	1800 ± 200		
100	240 ± 10	750 ± 40		
50	132 ± 8	350 ± 20	800 ± 70	
25	65 ± 3	183 ± 8	410 ± 30	
10	27 ± 2		150 ± 20	700 ± 200
5	11.8 ± 0.8		80 ± 10	240 ± 70

For laminar flow in a circular pipe, the ratio of v_{max}/v_{avg} is expected to be 2, where v_{max} is the maximum velocity and v_{avg} is the average velocity [45]. v_{avg} was found using $v_{avg} = \frac{Q}{A}$. Using the results for v_{max} obtained from the Ansys Fluent simulations, we find v_{max}/v_{avg} is equal to 2.08 in the simulations. This is not surprising considering that the simulations were done for a rectangular channel and not a circular pipe. The same ratio was calculated for the PIV data and is given in Table 3.4. We find the average value of v_{max}/v_{avg} from the experiments to be 2.2 ± 0.2 , which agrees with the simulations within the uncertainty.

The flow of Carbopol displayed a plug in the centre of the channel as seen in Figure 3.14b. This plug spanned two directions, across both the width and the height of the channel, giving a flow profile with a constant velocity for most of the channel but sharply dropping off at the channel edges. Within the plug, the Carbopol is unyielded, since the shear stress here is smaller than the

Table 3.4: v_{max}/v_{avg} of water in microfluidic channels derived from v_{max} measured for μ PIV and v_{avg} calculated from the flow rate and nominal channel dimensions.

Flow Rate (μ L/hr)	500 μ m (μ m/s)	300 μ m (μ m/s)	200 μ m (μ m/s)	100 μ m (μ m/s)
250	2.11	2.38		
100	2.14	2.44		
50	2.39	2.27	2.30	
25	2.37	2.37	2.36	
10	2.48		2.21	2.04
5	2.13		2.18	1.73

yield stress. A MATLAB code was written to find the average velocity in the plug region and the width of the plug by fitting a line to the plug as illustrated in Figure 3.15. The average of this line was taken to be the plug velocity, and the plug region was taken to be the region over which the velocity remained within 1 standard deviation of the fitted plug velocity. The plug velocities are shown as a function of flow rate for the different microchannels in Figure 3.16. For the 0.14 and 0.3 wt% concentrations, we find that the lightly mixed samples for a given concentration in a given channel at a given flow rate have lower average velocity in the plug region than the vigorously mixed. For the 1 wt% samples, while the plug velocities are similar between the two samples.

Liu et al. studied the flow for vigorously mixed 0.14 wt% Carbopol in 1 cm long square microchannels. In a 500 μ m channel, they measured a plug velocity of approximately 90 μ m/s for 55 μ L/hr and approximately 120 μ m/s for a flow rate of 70 μ L/hr [2]. In contrast, in a 500 μ m channel, we measured the plug velocity to be 63 ± 1 μ m/s for a flow rate of 50 μ L/hr and a plug velocity of 111.3 ± 0.3 μ m/s for a flow rate of 100 μ L/hr. There are differences between our fluids and our experimental methods. Our Carbopol has a yield stress of 12.9 ± 0.4 Pa, and Liu, et al.'s Carbopol had a yield stress of 10.5 ± 0.2 Pa. For the experiments here a computer controlled dual syringe pump ideally suited for creating extremely uniform and pulsation-free flow

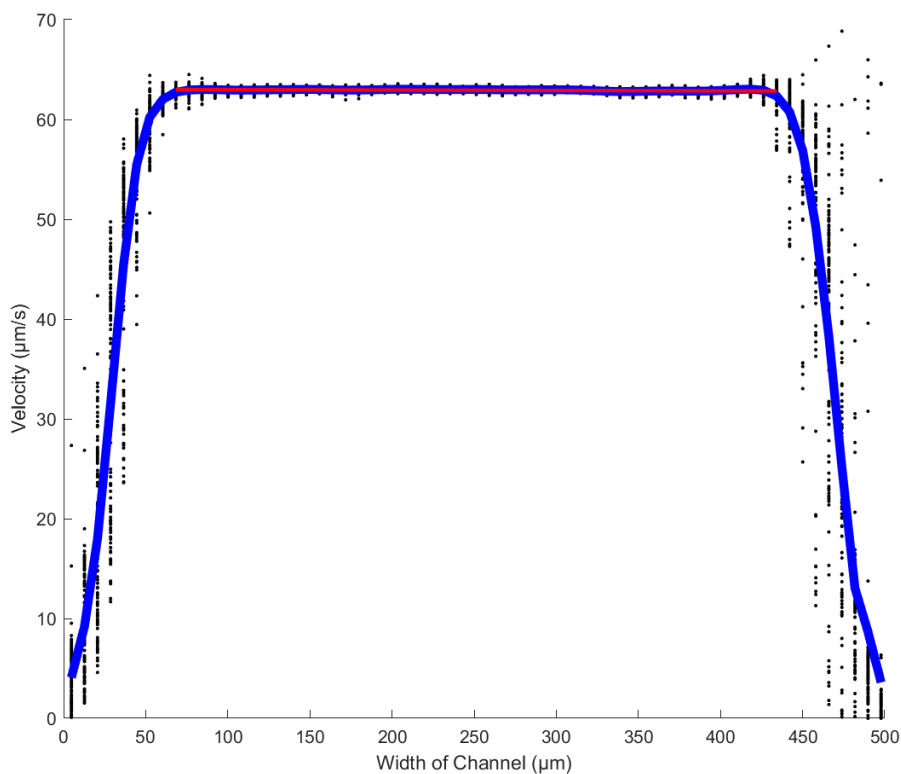


Figure 3.15: Flow profile of vigorously mixed 0.3 wt% Carbopol flowing at 50 $\mu\text{L/hr}$ in a 500 μm channel. The black points are the data, the blue line is the mean measured flow profile, and the red line is a straight line fit to the centre portion of the profile. The average of this straight line is taken as the plug velocity.

was used and the microchannel moulds were fabricated using a more precise milling procedure.

Table 3.5 gives the plug width averaged over the flow rates for each fluid in each channel. The width of the plug did not depend systematically on flow rate, nor did it depend on concentration, but it did depend on preparation method. The plugs observed in lightly mixed Carbopol were, on average, 13% wider than the vigorously mixed samples.

Similar experiments were performed with Medium BIS and High BIS 10 wt% PNIPAM as shown in Figure 3.17. PNIPAM was analyzed the same way as Carbopol, and the measured plug velocities were on the same order as Carbopol. Both samples were tested in a 300 μm channel. Here Medium BIS PNIPAM displayed a plug velocity approximately 20% greater

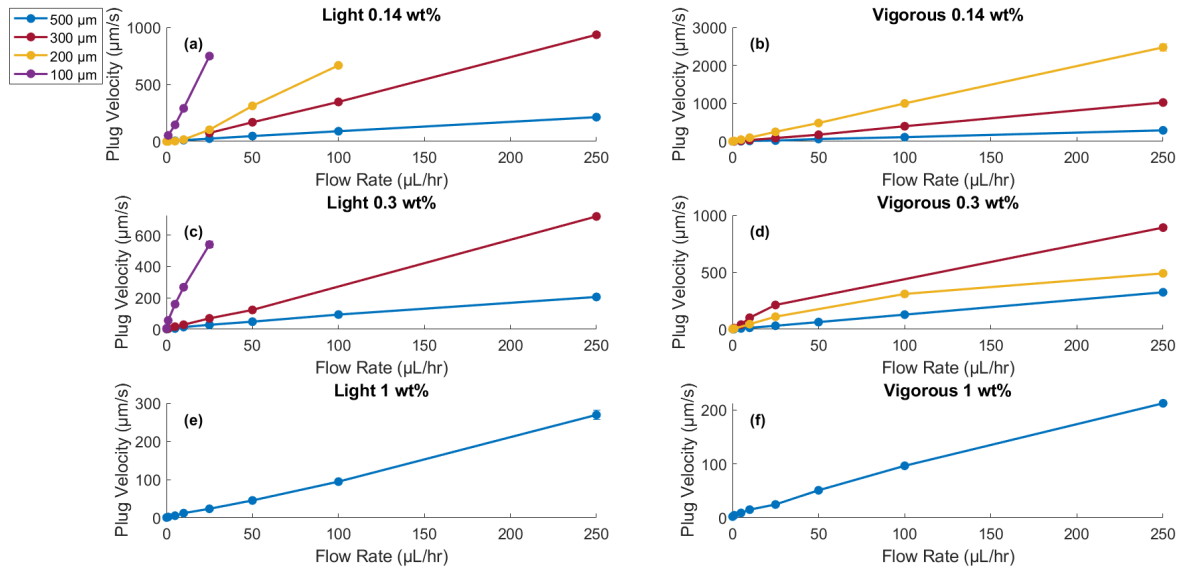


Figure 3.16: Average plug velocities of Carbopol samples in each channel at the mid-plane, approximately half way along the channel. a) lightly mixed 0.14 wt% Carbopol, b) vigorously mixed 0.14 wt% Carbopol, c) lightly mixed 0.3 wt% Carbopol, d) vigorously mixed 0.3 wt% Carbopol, e) lightly mixed 1 wt% Carbopol, f) vigorously mixed 1 wt% Carbopol.

than High BIS PNIPAM for flow rates above 25 µL/hr. At flow rates between 25 and 5 µL/hr, Medium BIS PNIPAM displayed a plug velocity approximately 50% lower than High BIS PNIPAM. At 1 µL/hr, Medium BIS PNIPAM displayed a plug velocity 72% lower than High BIS PNIPAM.

Like Carbopol, the plug width for PNIPAM remained fairly consistent across flow rates and showed no significant difference between the two samples used. The average plug width across flow rates are shown in Table 3.5. PNIPAM had a plug width similar to the lightly mixed Carbopol samples.

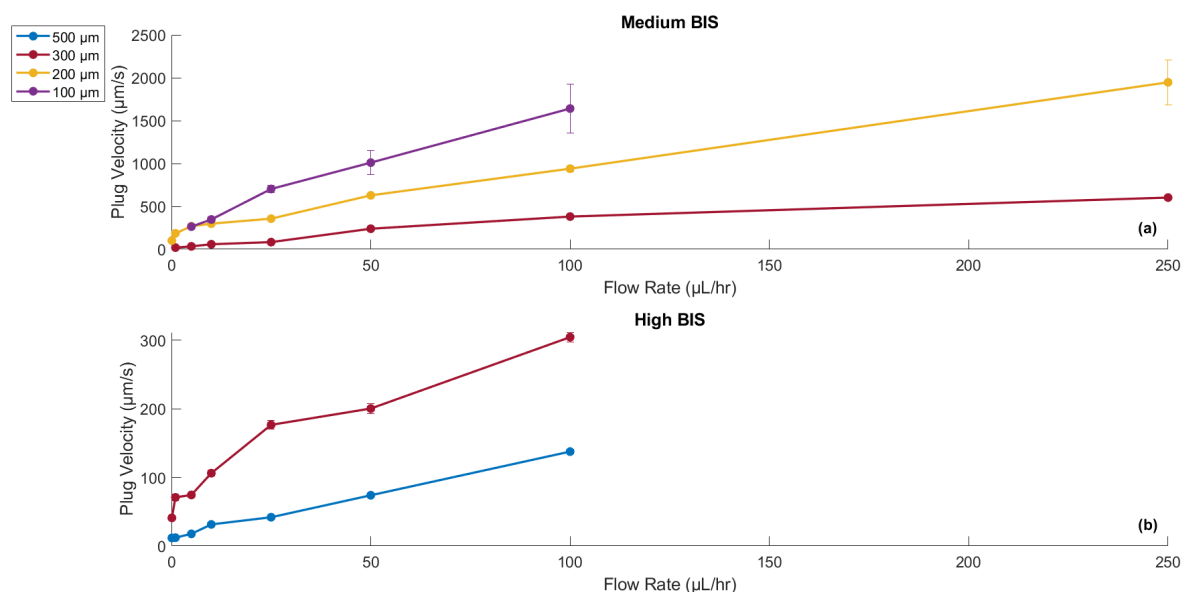


Figure 3.17: Average plug velocities of PNIPAM samples in each channel at the mid-plane, approximately half way along the channel. a) Medium BIS and b) High BIS.

Table 3.5: Width of plug averaged over flow rates displayed by Carbopol and PNIPAM samples at the mid-plane, approximately half way along the channel.

Sample	500 μm Plug Width (μm)	300 μm Plug Width (μm)	200 μm Plug Width (μm)	100 μm Plug Width (μm)
Carbopol				
0.14 wt%, light	460 \pm 20	220 \pm 5	144 \pm 9	71 \pm 2
0.14 wt%, vigorous	410 \pm 40	198 \pm 10	130 \pm 10	
0.3 wt%, light	470 \pm 10	248 \pm 6		91 \pm 6
0.3 wt%, vigorous	370 \pm 20	192 \pm 8	200 \pm 20	
1 wt%, light	430 \pm 40			
1 wt%, vigorous	400 \pm 40			
10 wt% PNIPAM				
Medium BIS		200 \pm 20	130 \pm 10	70 \pm 10
High BIS	320 \pm 20	180 \pm 10		
Average % of Channel Width	81%	69%	76%	77%

3.4.1 Analysis

Simulations of Carbopol and PNIPAM were attempted using Ansys Fluent. Fluent's implementation of the Herschel-Bulkley model is regularized by assuming a constant viscosity $\eta_r = \frac{\sigma_y}{\dot{\gamma}_r}$ for stresses lower than σ_y and shear rates lower than a user-specified critical shear rate, $\dot{\gamma}_r$. We found that the results of the simulations depended greatly on the choice of $\dot{\gamma}_r$ but did not have a dependence on yield stress. This was unexpected and clearly incorrect. In lieu of simulations we have fit the velocity profiles of Carbopol and PNIPAM to an equation by Escudier and Presti for the flow of a Herschel-Bulkley fluid in a circular pipe [46],

$$v(r) = \begin{cases} \frac{n}{n+1} \cdot \left(\frac{\sigma_w}{k}\right)^{\frac{1}{n}} \cdot \left(1 - \frac{\sigma_y}{\sigma_w}\right)^{\frac{n+1}{n}} - \left(\frac{r}{R} - \frac{\sigma_y}{\sigma_w}\right)^{\frac{n+1}{n}} & \text{if } r \gg \frac{\sigma_y}{\sigma_w} \cdot R \\ \frac{n}{n+1} \cdot \left(\frac{\sigma_w}{k}\right)^{\frac{1}{n}} \cdot R \cdot \left(1 - \frac{\sigma_y}{\sigma_w}\right)^{\frac{n+1}{n}} & \text{otherwise} \end{cases}, \quad (3.1)$$

where

- n = power law index from rheological experiments,
- σ_w = stress at the walls,
- k = consistency index from rheological experiments,
- R = $\frac{1}{2}$ channel width,
- σ_y = yield stress from rheological experiments,
- r = location within channel.

Values for the parameters of the fit to the Herschel-Bulkley model from Table 3.1 were used for σ_y , k , and n . σ_w was adjusted iteratively until v in the plug region matched the plug velocity found using μ PIV within 4 significant figures. σ_w was always greater than the yield stress, increased as channel size decreased, and increased as flow rate increased.

An example of a plot of equation 3.1 is shown in Figure 3.18 with the mean μ PIV data for Carbopol plotted overtop. The equation predicts a smaller plug region than that measured by

μ PIV. This difference is possibly a result of the equation being for a circular channel whereas the experiments were performed in square channels. Despite this, the experimentally measured velocity profile is qualitatively similar to that predicted by equation 3.1.

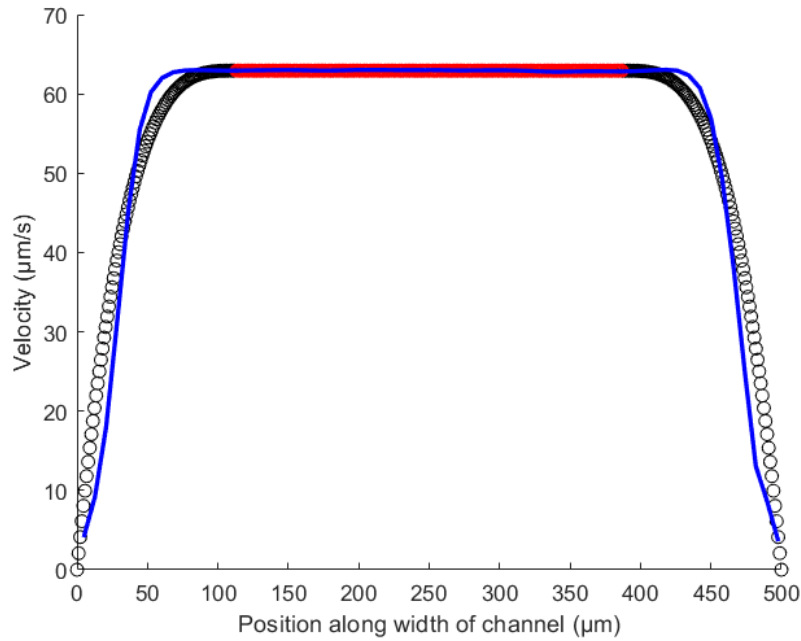


Figure 3.18: Plot of equation 3.1 for vigorously mixed 0.3 wt% Carbopol flowing at 50 $\mu\text{L/hr}$ in a 500 μm channel, overlaid with the mean μ PIV data. The black circles represent equation 3.1 when $r \gg \frac{\sigma_y}{\sigma_w} \cdot R$, the red circles represent the equation otherwise, and the blue line represents the μ PIV data.

A straight line was fit to a logarithmic plot of flow rate versus $\sigma_w - \sigma_y$. σ_y was adjusted manually so that the data appeared linear on this plot. Data for lightly mixed 0.14 wt% Carbopol in a 500 μm channel are shown in Figure 3.19. The best value of σ_y in this case was 4.7 ± 0.2 Pa. This is very close to the yield stress of 4.4 ± 0.1 Pa measured for this sample using the rheometer. The yield stress that gave the best fit for each sample are shown in Table 3.6. The slope of the fit is equal to the inverse of the power law index, n . The values of n obtained from the fit are shown in Table 3.7. There is no systematic variation in n with channel size. In the case of lightly mixed 0.14 wt% Carbopol there appears to be an increase in n in the smaller

channels, but it is necessary to observe more fluids in the smaller channels to make a definite conclusion.

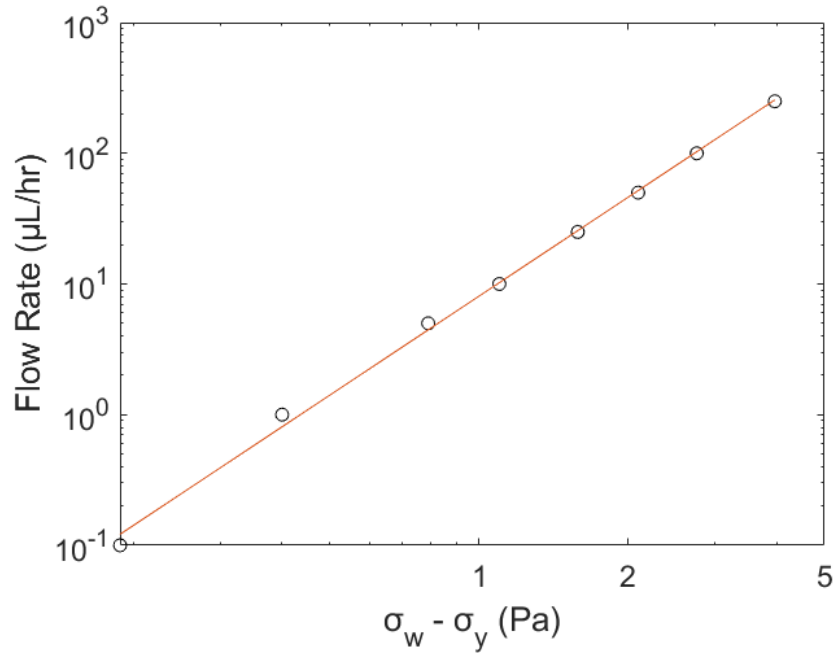


Figure 3.19: Logarithmic plot of flow rate versus $\sigma_w - \sigma_y$ lightly mixed 0.14 wt% Carbopol in a 500 μm channel using a yield stress of 4.7 Pa.

In the 500 and 300 μm channels, the yield stress found by fitting the μPIV data was always slightly higher than that found by the rheometer, but the results were consistent between the channels. In the 200 μm channel, lightly mixed 0.14 wt% Carbopol gave a yield stress consistent with the value found in the larger channels, vigorously mixed 0.14 wt% Carbopol gave a slightly higher yield stress than it did in the larger channels, and vigorously mixed 0.3 wt% Carbopol gave a yield stress slightly lower than it did in the larger channels. There was, however, a significant increase in yield stress in the 100 μm channel from that found in the larger channels. Lightly mixed 0.14 wt% Carbopol was 68% larger, and lightly mixed 0.3 wt% Carbopol was 35% larger in the 100 μm channel than in the larger channels. Jofore et al. [20]

Table 3.6: Yield stresses that resulted in the best fit for a logarithmic plot of $\sigma_w - \sigma_y$ vs. flow rate.

Sample	Rheometer σ_y (Pa)	500 μm σ_y (Pa)	300 μm σ_y (Pa)	200 μm σ_y (Pa)	100 μm σ_y (Pa)
Carbopol					
light 0.14 wt%	4.4 ± 0.1	4.7 ± 0.2	4.7 ± 0.2	4.7 ± 0.2	7.9 ± 0.4
vigorous 0.14 wt%	12.9 ± 0.4	13.0 ± 0.8	13.9 ± 0.3	15.1 ± 0.3	
light 0.3 wt%	9.57 ± 0.08	11.2 ± 0.2	11.0 ± 0.5		15 ± 2
vigorous 0.3 wt%	18.8 ± 0.1	20 ± 2	10 ± 10	8 ± 8	
light 1 wt%	24.6 ± 0.2	27.4 ± 0.4			
vigorous 1 wt%	104 ± 0.2	126 ± 2			
10 wt% PNIPAM at 20 °C					
Medium BIS	38 ± 2	63 ± 3	30 ± 30		
High BIS	13 ± 1		36 ± 2	75 ± 5	60 ± 60

and Yan et al. [21] also found an increase in yield stress of Carbopol in confined geometries, in agreement with the present results. Liu, et al., on the other hand, who performed similar microchannel experiments, found a decrease in yield stress of Carbopol when it was confined to channels smaller than 150 μm [2], which was consistent with work by Geraud, et al. [13].

A similar analysis was carried out for the μPIV data obtained with PNIPAM flowing in the microchannels. In contrast to what was found for Carbopol, there was no change in yield stress between the 200 and 100 μm channel as shown in Table 3.6. This is expected since, as seen in our dynamic light scattering data, PNIPAM has a significantly smaller particle size than Carbopol. In a 100 μm channel, vigorously mixed Carbopol has a mean particle size to channel size ratio of 1.9×10^{-1} and lightly mixed Carbopol has a ratio of 4×10^{-2} . PNIPAM, on the other hand, has a particle size to channel size ratio of 1.4×10^{-3} for Medium BIS PNIPAM and 1.9×10^{-3} for High BIS PNIPAM.

Table 3.7: Inverse of slope values of a logarithmic plot of flow rate versus $\sigma_w - \sigma_y$, which is equivalent to the power law index, n .

Sample	Rheometer n	500 μm n	300 μm n	200 μm n	100 μm n
Carbopol					
light 0.14 wt%	0.48 ± 0.01	0.40 ± 0.08	0.48 ± 0.07	0.9 ± 0.1	0.69 ± 0.08
vigorous 0.14 wt%	0.42 ± 0.02	0.28 ± 0.05	0.43 ± 0.04	0.44 ± 0.03	
light 0.3 wt%	0.458 ± 0.003	0.46 ± 0.06	0.36 ± 0.04		0.40 ± 0.06
vigorous 0.3 wt%	0.424 ± 0.002	0.36 ± 0.06	0.21 ± 0.04	0.20 ± 0.04	
light 1 wt%	0.488 ± 0.003	0.47 ± 0.02			
vigorous 1 wt%	0.377 ± 0.007	0.44 ± 0.03			
10 wt% PNIPAM at 20 °C					
Medium BIS	0.424 ± 0.006	0.47 ± 0.09	0.14 ± 0.04		
High BIS	0.377 ± 0.006		0.48 ± 0.03	0.35 ± 0.03	0.3 ± 0.1

Chapter 4

Discussion and Conclusions

In this thesis we have presented the measurements of the rheological behaviour and particle size of Carbopol and PNIPAM. We have also presented a study of the flow of water, Carbopol, and PNIPAM in square microchannels. The flow of water was simulated using Ansys Fluent. The flow of Carbopol and PNIPAM was analyzed using an equation for laminar flow of a Herschel-Bulkley fluid in a circular pipe [46].

Dynamic light scattering was used to characterize the particle size of Carbopol and PNIPAM. The measurements revealed that increasing mixing time decreased the mean particle size and polydispersity of Carbopol. This is in agreement with the work of Dinkgreve, et al. and Lee, et al, who both found that increasing mixing time decreases the particle size of Carbopol [12,23]. The measurements also revealed that PNIPAM has a mean particle size on the order of 100 nanometers, significantly smaller than Carbopol which has a mean particle size of a few micrometers. Increasing the crosslinker concentration of PNIPAM was shown to decrease the mean particle size and polydispersity. This is in agreement with the work done by Senff and Richtering [16]

We performed four rheological tests on Carbopol: flow curves, amplitude sweeps, frequency

sweeps, and creep tests. The flow curves showed that the yield stress of vigorously mixed samples was significantly larger than the yield stress of lightly mixed samples. Flow curves were measured for both increasing and decreasing shear rates. 0.3 wt% and lightly mixed 1 wt% Carbopol samples showed no hysteresis, however 0.14 wt% and vigorously mixed 1 wt% Carbopol did. Although Carbopol is widely regarded as a simple yield-stress fluid with no hysteresis [33–40], studies have shown that Carbopol does not always behave as a simple yield-stress fluid and can display hysteresis [41]. Dinkgreve, et al., using a different form of Carbopol (Ultrez U10), found that vigorously mixed samples showed hysteresis but lightly mixed did not [23]. The emergence of hysteresis in our data could be attributed to differences in the type of Carbopol used and differences in preparation method.

All amplitude and frequency sweeps were in excellent agreement with previous measurements on Carbopol [10, 11]. We determined the yield stress of Carbopol samples using creep tests. The yield stresses determined from the creep tests were in good agreement with those determined from the flow curves.

Three samples of PNIPAM were prepared using the compositions in Table 2.1. Increasing and decreasing flow curves were also performed on 10 wt% PNIPAM at temperatures ranging from 5°C to 40 °C. The flow curves for Low BIS PNIPAM did not have much curvature, making it hard to fit the data to the Herschel-Bulkley model. Medium and High BIS PNIPAM showed a decrease in yield stress and consistency index as temperature increased, while the power law index remained relatively constant. This decrease in yield stress is due to the increase in particle size that occurs as PNIPAM is heated.

The viscosity of PNIPAM was measured at a fixed shear rate as a function of temperature. Viscosity decreased linearly with temperature until around 25°C where there was a change in slope and a nonlinear temperature dependence. Above 33°C, the LCST, the viscosity ap-

proached a constant value. Low BIS PNIPAM displayed the highest viscosity at low temperatures and High BIS PNIPAM displayed the lowest viscosity. This correlates to High BIS PNIPAM having a smaller mean particle size than Medium BIS PNIPAM and the particle size of each decreasing as the temperature increases. At a given concentration, smaller particles are further apart in the solution resulting in weaker hydrodynamic interactions and less dissipation. The result is a smaller viscosity.

Flow of water in 1 cm long square microchannels ranging in width from 100 μm to 500 μm was simulated using Ansys Fluent. The simulation results for water were as expected, with an approximately parabolic profile and the maximum velocity increasing with channel size and with flow rate. The ratio v_{max}/v_{avg} was consistently equal to 2.08. For laminar flow in a circular pipe, the ratio of v_{max}/v_{avg} is expected to be 2. This difference is not surprising considering we used square and not circular channels.

Using micro-particle image velocimetry, the flow of the fluids was visualized in 1 cm long square microchannels ranging in width from 100 μm to 500 μm . These experiments improved on previous work by Liu, et al. [2] by using new microchannel moulds that were manufactured using a more precise milling machine giving smoother channels, a computer controlled dual syringe pump giving more accurate and pulsation-free flow rates, and by taking velocimetry measurements at multiple heights throughout the channel giving a quasi-three-dimensional measurement of the flow profile.

Velocity profiles measured for water were approximately parabolic and the maximum velocity increased linearly with flow rate and with channel size as expected. Experimental velocity profiles of water had an average v_{max}/v_{avg} of 2.2 ± 0.2 . This agrees with those of the simulations. The fact that the experimental results for water were in agreement with our simulations, and that both displayed the expected dependence on channel size and flow rate, gives us confidence

that our experimental and analysis methods are accurate.

The velocity profiles for Carbopol and PNIPAM displayed a plug in the centre of the channel, as expected for a yield-stress fluid [47]. For 0.14 and 0.3 wt%, vigorously mixed Carbopol samples had greater average velocities in the plug region than the lightly mixed. Meanwhile the 1 wt% Carbopol samples showed similar plug velocities. Using the same type of Carbopol, Liu et al. studied vigorously mixed 0.14 wt% Carbopol in 1 cm long square microchannels. In a 500 μm channel, they measured a plug velocity of approximately 90 $\mu\text{m/s}$ for a flow rate of 55 $\mu\text{L/hr}$ and approximately 120 $\mu\text{m/s}$ for a flow rate of 70 $\mu\text{L/hr}$ [2]. In contrast, in a 500 μm channel we measured the plug velocity to be 63 ± 1 $\mu\text{m/s}$ for a flow rate of 50 $\mu\text{L/hr}$ and 111.3 ± 0.3 $\mu\text{m/s}$ for a flow rate of 100 $\mu\text{L/hr}$.

There is a difference in yield stress between our Carbopol and that of Liu, et al. Our 0.14 wt% vigorously mixed Carbopol had a yield stress of 12.9 ± 0.4 Pa while the sample used by Liu, et al. displayed a yield stress of 10.5 ± 0.2 Pa. This may at least partly explain the difference in measured plug velocities. Oddly though, we found that the plug velocity of 0.14 and 0.3 wt% Carbopol, for a given flow rate in a given channel, increased as yield stress increased. The difference in the plug velocity measured by Liu, et al and the work here may also be partly due to differences in experimental procedures. Since the work done by Liu, et al. we have made several improvements to our experimental methods. A computer controlled syringe pumps ideally suited for creating extremely uniform and pulsation-free flow was used. In addition, the microchannel moulds were fabricated using a more precise milling procedure.

For our experimental conditions, the average plug width measured for Carbopol did not depend on concentration, but it did depend on preparation method. On average, the plug width measured for lightly mixed Carbopol was 13% larger than the width measured for vigorously mixed Carbopol. This difference is consistent with the difference measured in yield stress: the

lightly mixed samples have a lower yield stress than the vigorously mixed samples of the same concentration. Oddly, this is the opposite of what we expect for a correlation between plug width and yield stress.

Medium and High BIS PNIPAM were used in μ PIV experiments. Both samples displayed plug velocities on the same order as those observed in Carbopol. Like Carbopol, the width of the plug for PNIPAM remained fairly consistent as a function of flow rates and no significant difference between the two samples was observed. The plug width measured for PNIPAM was similar to that measured for lightly mixed Carbopol samples.

In lieu of simulations we fit the velocity profiles of Carbopol and PNIPAM to an equation by Escudier and Presti for the flow of a Herschel-Bulkley fluid in a circular pipe [46]. In the larger channels, fitting a straight line to a logarithmic plot of flow rate versus $\sigma_w - \sigma_y$ by manually adjusting σ_y gave a σ_y slightly higher than the yield stress found by fitting the Herschel-Bulkley model to flow curve measurements. For Carbopol in a 100 μm channel using this method the yield stress is significantly higher than it is for the same sample in larger channels. This change may be due to effects of confinement becoming significant in the 100 μm channel. If so, this would indicate that Carbopol begins to display confinement effects when the width of the channel is between the 200 and 100 μm . This agrees with the work by Liu, et al who observed confinement effects in square microchannels below 150 μm in width [2]. We observed an increase in yield stress in the 100 μm channel, which is in direct opposition to the measurements by Liu, et al. [2] and Geraud et al. [13], but in a agreement with some other studies on confinement [20,21].

Using the analysis method with equation 3.1, a change in the yield stress was not observed for PNIPAM in the channels studied. This is presumably due to the fact that the PNIPAM particles are still much smaller than the channel width, even in the smallest channels studied.

Unfortunately due to the COVID-19 pandemic my time in the lab was cut short and I was unable to perform μ PIV experiments on all fluids in all the channels. In order to make a strong conclusion about confinement effects I would have collected data for all my fluids in 100 and 50 μm channels.

Manufacturing 50 μm channels using our soft lithography method proved to be a challenge. It is unlikely that quality 50 μm channels are possible using current soft lithography methods, however, they are possible using photolithography. Based on the data we do have, it is expected that confinement effects would be present for all Carbopol samples, but not PNIPAM, in both 100 and 50 μm channels. We were able, with the data collected, to see a dependence on the concentration of Carbopol used and its preparation method.

In the future, to understand confinement effects all concentrations and preparation methods of Carbopol and PNIPAM should be studied in smaller microchannels. To further understand the polydispersity of the fluids, fluorescent confocal microscopy could be used for imaging. It would be interesting to see how temperature affects the flow of PNIPAM in microchannels. Temperature-controlled microchannels could be fabricated using a method called microwiring. PDMS would be cured around three parallel microwires at very small intervals. Two of the microwires would be removed, the middle one and one on the edge. Flow would happen in the middle channel while nitrogen is blown through the other hollow channel to cool the channel. The remaining microwire would be connected to an electrical source to heat the microchannel.

Overall, in this thesis we have characterized the rheology and particle size of Carbopol and PNIPAM and their flow when injected into microchannels. We demonstrated that preparation method has an effect on the properties of Carbopol in all the experimental methods used. We also demonstrated that the crosslinker (BIS) concentration used for the synthesis on PNIPAM

has an effect on its viscosity and particle size. Our μ PIV experiments provided some evidence that Carbopol begins to display confinement effects in square microchannels less than 200 μm in width, although the increase in yield stress observed in our experiments is different from the decrease in yield stress observed in previous microchannel flow experiments conducted in our laboratory. We did not observe confinement effects in PNIPAM, indicating that confinement effects are dependent on particle size. It would be beneficial to perform similar experiments with these fluids in smaller channels to further quantify confinement effects.

Bibliography

- [1] Anton Paar. Modular Compact Rheometer: MCR xx2. <https://www.anton-paar.com/ca-en/products/details/rheometer-mcr-102-302-502/dmta/>. Accessed: 2020-04-28.
- [2] Yang Liu, Daniel Lorusso, David W Holdsworth, Tamie L Poepping, and John R de Bruyn. Effect of confinement on the rheology of a yield-stress fluid. *Journal of Non-Newtonian Fluid Mechanics*, 261:25–32, 2018.
- [3] H.A. Barnes, J.F. Hutton, and K. Walters. *An Introduction to Rheology*. Elsevier, 1989.
- [4] Ronald Darby. *Viscoelastic Fluids*. Marcel Dekker, Inc., 1976.
- [5] Piaras Kelly. Solid mechanics part i: An introduction to solid mechanics: Viscoelasticity. http://homepages.engineering.auckland.ac.nz/~pkel015/SolidMechanicsBooks/Part_I/index.html.
- [6] Ronald G. Larson. *The Structure and Rheology of Complex Fluids*. Oxford University Press, 1999.
- [7] Anonymous. Silly Putty. <http://www.physics.usyd.edu.au/cross/SILLYPUTTY.htm>.
- [8] The University of Auckland. Rheological Models. http://homepages.engineering.auckland.ac.nz/~pkel015/SolidMechanicsBooks/Part_I/BookSM_Part_I/10_Viscoelasticity/10_Viscoelasticity_03_Rheological.pdf. Accessed: 2018-06-02.

- [9] Anton Paar. Basics of Thixotropy. <https://wiki.anton-paar.com/ca-en/basics-of-thixotropy/>. Accessed: 2020-04-21.
- [10] Priscilla R Vargas, Camila M Costa, Bruno S Fonseca, Mônica F Naccache, and Paulo R de Souza Mendes. Rheological characterization of carbopol® dispersions in water and in water/glycerol solutions. *Fluids*, 4(1):3, 2019.
- [11] E Di Giuseppe, F Corbi, F Funicello, A Massmeyer, TN Santimano, M Rosenau, and A Davaille. Characterization of carbopol® hydrogel rheology for experimental tectonics and geodynamics. *Tectonophysics*, 642:29–45, 2015.
- [12] David Lee, Iris A Gutowski, Arthur E Bailey, Laurent Rubatat, John R de Bruyn, and Barbara J Frisken. Investigating the microstructure of a yield-stress fluid by light scattering. *Physical Review E*, 83(3):031401, 2011.
- [13] Baudouin Geraud, Lyderic Bocquet, and Catherine Barentin. Confined flows of a polymer microgel. *The European Physical Journal E*, 36(3):30, 2013.
- [14] Lubrizol Technical Data Sheet. Molecular weight of carbopol and pemulen polymers, 2007.
- [15] FK Oppong and JR de Bruyn. Microrheology and jamming in a yield-stress fluid. *Rheologica acta*, 50(4):317–326, 2011.
- [16] Holger Senff and Walter Richtering. Influence of cross-link density on rheological properties of temperature-sensitive microgel suspensions. *Colloid and Polymer Science*, 278(9):830–840, 2000.
- [17] H Senff and W Richtering. Temperature sensitive microgel suspensions: Colloidal phase behavior and rheology of soft spheres. *The Journal of chemical physics*, 111(4):1705–1711, 1999.

- [18] Brian R Saunders. On the structure of poly (n-isopropylacrylamide) microgel particles. *Langmuir*, 20(10):3925–3932, 2004.
- [19] Irmgard Bischofberger and Veronique Trappe. New aspects in the phase behaviour of poly-n-isopropyl acrylamide: systematic temperature dependent shrinking of pnipam assemblies well beyond the lcst. *Scientific reports*, 5:15520, 2015.
- [20] Bruke Daniel Jofore, Philipp Erni, Giovanni Vleminckx, Paula Moldenaers, and Christian Clasen. Rheology of microgels in single particle confinement. *Rheologica Acta*, 54(7):581–600, 2015.
- [21] Y Yan, Z Zhang, D Cheneler, JR Stokes, and MJ Adams. The influence of flow confinement on the rheological properties of complex fluids. *Rheologica acta*, 49(3):255–266, 2010.
- [22] Yang Liu. *Three Experiments on Complex Fluids*. PhD thesis, University of Western Ontario, 2017.
- [23] M Dinkgreve, M Fazilati, MM Denn, and Daniel Bonn. Carbopol: From a simple to a thixotropic yield stress fluid. *Journal of Rheology*, 62(3):773–780, 2018.
- [24] University of Texas. ALV/CGS-3 Dynamic Light Sacttering. <http://www.caee.utexas.edu/prof/saleh/facilities1.html>. Accessed: 2020-04-07.
- [25] Stephen W Provencher. Contin: a general purpose constrained regularization program for inverting noisy linear algebraic and integral equations. *Computer Physics Communications*, 27(3):229–242, 1982.
- [26] A Scotti, W Liu, JS Hyatt, ES Herman, HS Choi, JW Kim, LA Lyon, U Gasser, and A Fernandez-Nieves. The contin algorithm and its application to determine the size distribution of microgel suspensions. *The Journal of Chemical Physics*, 142(23):234905, 2015.

- [27] Iari-Gabriel Marino. rilt. <https://www.mathworks.com/matlabcentral/fileexchange/6523-rilt>. Accessed: 2020-05-21.
- [28] Anonymous. SOLIDWORKS 3D CAD. <https://www.solidworks.com/product/solidworks-3d-cad>. Accessed: 2020-04-30.
- [29] Anonymous. Mastercam. <https://www.mastercam.com/>. Accessed: 2020-04-30.
- [30] Ansys Fluent. Ansys Free Student Software Downloads. <https://www.ansys.com/academic/free-student-products>. Accessed: 2020-04-30.
- [31] Anonymous. Low Pressure Syringe Pump neMESYS 290N. <https://www.cetoni.com/products/low-pressure-syringe-pump-nemesys-290n/>. Accessed: 2020-04-30.
- [32] LaVision Inc. DaVis – Software Solution for Intelligent Imaging. <https://www.lavision.de/en/products/davis-software/>. Accessed: 2020-04-30.
- [33] Jong-Yun Kim, Jun-Yeob Song, Eun-Joo Lee, and Seung-Kyu Park. Rheological properties and microstructures of carbopol gel network system. *Colloid and Polymer Science*, 281(7):614–623, 2003.
- [34] Philippe Coussot, Laurent Tocquer, C Lanos, and Guillaume Ovarlez. Macroscopic vs. local rheology of yield stress fluids. *Journal of Non-Newtonian Fluid Mechanics*, 158(1-3):85–90, 2009.
- [35] Steven P Meeker, Roger T Bonnecaze, and Michel Cloitre. Slip and flow in soft particle pastes. *Physical Review Letters*, 92(19):198302, 2004.
- [36] Julie Goyon, Annie Colin, G Ovarlez, A Ajdari, and L Bocquet. Spatial cooperativity in soft glassy flows. *Nature*, 454(7200):84–87, 2008.

- [37] BW Barry and MC Meyer. The rheological properties of carbopol gels i. continuous shear and creep properties of carbopol gels. *International journal of pharmaceutics*, 2(1):1–25, 1979.
- [38] B.W. Barry and M.C. Meyer. Carbopol gels: Elastoviscoplastic and slippery glasses made of individual swollen sponges: Meso-and macroscopic properties, constitutive equations and scaling laws. *Journal of non-newtonian fluid mechanics*, 144(1):1–29, 2007.
- [39] Philippe Coussot and F Gaulard. Gravity flow instability of viscoplastic materials: The ketchup drip. *Physical Review E*, 72(3):031409, 2005.
- [40] Philippe Coussot, Laurent Tocquer, C Lanos, and Guillaume Ovarlez. Macroscopic vs. local rheology of yield stress fluids. *Journal of Non-Newtonian Fluid Mechanics*, 158(1-3):85–90, 2009.
- [41] AMV Putz, TI Burghilea, IA Frigaard, and DM Martinez. Settling of an isolated spherical particle in a yield stress shear thinning fluid. *Physics of Fluids*, 20(3):033102, 2008.
- [42] Srinivasa R Raghavan, Li Ang Chen, Christopher McDowell, Saad A Khan, Robin Hwang, and Scott White. Rheological study of crosslinking and gelation in chlorobutyl elastomer systems. *Polymer*, 37(26):5869–5875, 1996.
- [43] Michael Gasik, Ana Gantar, Saša Novak, et al. Viscoelastic behaviour of hydrogel-based composites for tissue engineering under mechanical load. *Biomedical materials*, 12(2):025004, 2017.
- [44] D CH Cheng. Yield stress: a time-dependent property and how to measure it. *Rheologica Acta*, 25(5):542–554, 1986.
- [45] James C.Y. Guo. Theoretical fluid mechanics: Laminar flow velocity profile. <https://www.ucdenver.edu/faculty-staff/jguo/Documents/Fluid1/11Laminar.pdf>.

- [46] MP Escudier and F Presti. Pipe flow of a thixotropic liquid. *Journal of Non-Newtonian Fluid Mechanics*, 62(2-3):291–306, 1996.
- [47] P. Coussot. Yield stress fluid flows: a review of experimental data. <http://philippecoussot.com/wp-content/uploads/2015/02/Article-135.pdf>. Accessed: 2020-08-02.

Appendix A

MATLAB Codes

pivplot3Davg.m

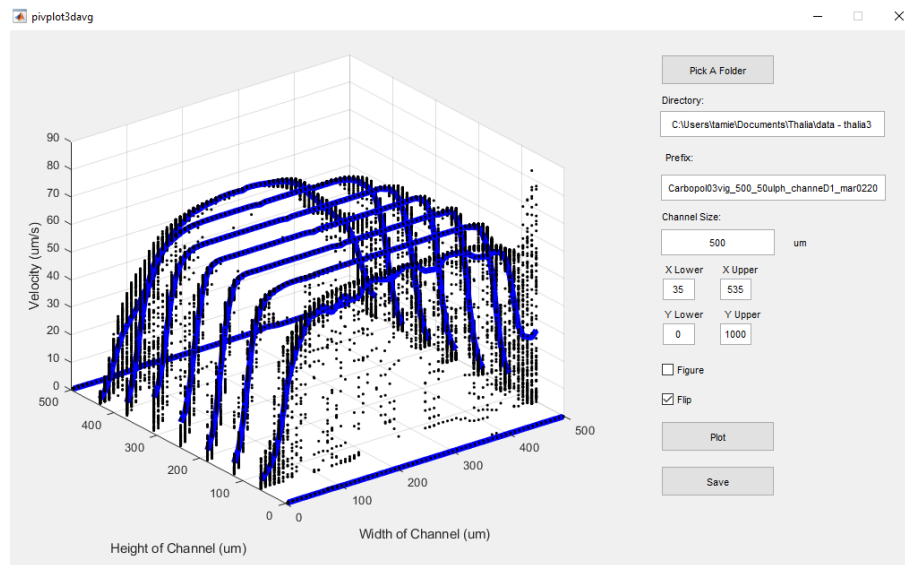


Figure A.1: pivplot3Davg.m GUI.

The program pivplot3Davg.m was used to obtain the flow profiles shown in Figure 3.14. The program pivplot3Davg.m is a graphical user interface (GUI) that imports text files that have been exported by LaVision's DaVis software, converts it into a format that MATLAB will plot, and plots a three-dimensional graph of velocity, height, and width of the channel. The velocity

and the width come from the data exported from Davis. The height, on the other hand, is set to increase from zero in increments of the channel width divided by the number of slices, nine, so that the final height is the same as the channel width. Upon pressing the save button the figure is saved in multiple formats, as the figure as seen on the GUI, as only the average velocity values, as a surface plot, and as individual plots of the average velocity for each slice.

```

1 function varargout = pivplot3davg(varargin)
2 % PIVPLOT3DAVG MATLAB code for pivplot3davg.fig
3 %     PIVPLOT3DAVG, by itself, creates a new PIVPLOT3DAVG or raises the existing
4 %     singleton*.
5 %
6 %     H = PIVPLOT3DAVG returns the handle to a new PIVPLOT3DAVG or the handle to
7 %     the existing singleton*.
8 %
9 %     PIVPLOT3DAVG('CALLBACK',hObject,eventData,handles,...) calls the local
10 %    function named CALLBACK in PIVPLOT3DAVG.M with the given input arguments.
11 %
12 %     PIVPLOT3DAVG('Property','Value',...) creates a new PIVPLOT3DAVG or raises the
13 %    existing singleton*. Starting from the left, property value pairs are
14 %    applied to the GUI before pivplot3davg_OpeningFcn gets called. An
15 %    unrecognized property name or invalid value makes property application
16 %    stop. All inputs are passed to pivplot3davg_OpeningFcn via varargin.
17 %
18 %    *See GUI Options on GUIDE's Tools menu. Choose "GUI allows only one
19 %    instance to run (singleton)".
20 %
21 % See also: GUIDE, GUIDATA, GUIHANDLES
22
23 % Edit the above text to modify the response to help pivplot3davg
24
25 % Last Modified by GUIDE v2.5 30-Mar-2020 16:01:45
26
27 % Begin initialization code - DO NOT EDIT
28 gui_Singleton = 1;
29 gui_State = struct('gui_Name',       mfilename, ...
30                  'gui_Singleton',   gui_Singleton, ...
31                  'gui_OpeningFcn', @pivplot3davg_OpeningFcn, ...
32                  'gui_OutputFcn',  @pivplot3davg_OutputFcn, ...
33                  'gui_LayoutFcn',  [] , ...
34                  'gui_Callback',    []);

```

```

35 if nargin && ischar(varargin{1})
36     gui_State.gui_Callback = str2func(varargin{1});
37 end
38
39 if nargin
40     [varargout{1:nargout}] = gui_mainfcn(gui_State, varargin{:});
41 else
42     gui_mainfcn(gui_State, varargin{:});
43 end
44 % End initialization code - DO NOT EDIT
45
46 % --- Executes just before pivplot3davg is made visible.
47 function pivplot3davg_OpeningFcn(hObject, eventdata, handles, varargin)
48 handles.output = hObject;
49 set(handles.folder, 'String', 'C:\Users\tamie\Documents\Thalia\data - thalia3');
50 guidata(hObject, handles);
51
52 % --- Outputs from this function are returned to the command line.
53 function varargout = pivplot3davg_OutputFcn(hObject, eventdata, handles)
54 varargout{1} = handles.output;
55
56 % --- Executes on button press in pickafolder.
57 function pickafolder_Callback(hObject, eventdata, handles)
58 path = uigetdir;
59 set(handles.folder, 'String', path);
60
61 function folder_Callback(hObject, eventdata, handles)
62 set(handles.folder, 'String', get(hObject, 'String'));
63 guidata(hObject, handles);
64
65 % --- Executes during object creation, after setting all properties.
66 function folder_CreateFcn(hObject, eventdata, handles)
67 if ispc && isequal(get(hObject, 'BackgroundColor'), get(0, 'defaultUicontrolBackgroundColor'))
68     set(hObject, 'BackgroundColor', 'white');
69 end
70
71 function prefix_Callback(hObject, eventdata, handles)
72 set(handles.prefix, 'String', get(hObject, 'String'));
73 guidata(hObject, handles);
74
75 % --- Executes during object creation, after setting all properties.

```

```
76 function prefix_CreateFcn(hObject, eventdata, handles)
77 if ispc && isequal(get(hObject,'BackgroundColor'), get(0,'defaultUicontrolBackgroundColor'))
78     set(hObject,'BackgroundColor','white');
79 end
80
81 function channelsize_Callback(hObject, eventdata, handles)
82 set(handles.channelsize, 'String', get(hObject, 'String'));
83 guidata(hObject, handles);
84
85 % --- Executes during object creation, after setting all properties.
86 function channelsize_CreateFcn(hObject, eventdata, handles)
87 if ispc && isequal(get(hObject,'BackgroundColor'), get(0,'defaultUicontrolBackgroundColor'))
88     set(hObject,'BackgroundColor','white');
89 end
90
91 function xlower_Callback(hObject, eventdata, handles)
92 set(handles.xlower, 'String', get(hObject, 'String'));
93 guidata(hObject, handles);
94
95 % --- Executes during object creation, after setting all properties.
96 function xlower_CreateFcn(hObject, eventdata, handles)
97 if ispc && isequal(get(hObject,'BackgroundColor'), get(0,'defaultUicontrolBackgroundColor'))
98     set(hObject,'BackgroundColor','white');
99 end
100
101 function xupper_Callback(hObject, eventdata, handles)
102 set(handles.xupper, 'String', get(hObject, 'String'));
103 guidata(hObject, handles);
104
105 % --- Executes during object creation, after setting all properties.
106 function xupper_CreateFcn(hObject, eventdata, handles)
107 if ispc && isequal(get(hObject,'BackgroundColor'), get(0,'defaultUicontrolBackgroundColor'))
108     set(hObject,'BackgroundColor','white');
109 end
110
111 function ylower_Callback(hObject, eventdata, handles)
112 set(handles.ylower, 'String', get(hObject, 'String'));
113 guidata(hObject, handles);
114
115 % --- Executes during object creation, after setting all properties.
116 function ylower_CreateFcn(hObject, eventdata, handles)
```

```

117 if ispc && isequal(get(hObject,'BackgroundColor'), get(0,'defaultUicontrolBackgroundColor'))
118     set(hObject,'BackgroundColor','white');
119 end
120
121 function yupper_Callback(hObject, eventdata, handles)
122 set(handles.yupper, 'String', get(hObject, 'String'));
123 guidata(hObject, handles);
124
125 % --- Executes during object creation, after setting all properties.
126 function yupper_CreateFcn(hObject, eventdata, handles)
127 if ispc && isequal(get(hObject,'BackgroundColor'), get(0,'defaultUicontrolBackgroundColor'))
128     set(hObject,'BackgroundColor','white');
129 end
130
131 % --- Executes on button press in figure_check.
132 function figure_check_Callback(hObject, eventdata, handles)
133
134 % --- Executes on button press in flip.
135 function flip_Callback(hObject, eventdata, handles)
136
137 % --- Executes on button press in plotbutton.
138 function plotbutton_Callback(hObject, eventdata, handles)
139 tic
140 'Plotting...'
141 cla
142 path = get(handles.folder, 'String');
143 prefix = get(handles.prefix, 'String');
144 dirinfo = dir(path);
145 dirinfo(~[dirinfo.isdir]) = []; %remove non-directories
146 count = 0;
147 for K = 1 : length(dirinfo)
148     thisdir = dirinfo(K).name;
149     if startsWith(thisdir, prefix) == 1
150         count = count + 1;
151         subdirinfo{count} = dir(fullfile(path, thisdir, '*.txt'));
152         foldernames{count} = thisdir;
153     end;
154 end
155
156 for i = 1:length(subdirinfo)
157     files(i,:) = {subdirinfo{1}.name};

```

```

158 end;
159
160 [numfolders numfiles] = size(files);
161
162 for j = 1:numfolders % typically 9
163     for u = 1:numfiles %typically 9
164         fullfilename = [path '\' char(foldernames{j}) '\' char(files(j,u))];
165         % Read file in as a series of strings
166         fid = fopen(fullfilename, 'rb');
167         strings = textscan(fid, '%s', 'Delimiter', '');
168         fclose(fid);
169
170         % Replace all commas with decimal points
171         decimal_strings = regexp(strings{1}, ',', '.');
172
173         % Convert to doubles and join all rows together
174         data = cellfun(@str2num, decimal_strings, 'uni', 0);
175         data = cat(1, data{:});
176
177         % Store data in array
178         alldata(j,u) = {data};
179
180         % Convert to matrix
181         datamat = cell2mat({data});
182
183         % Get x and y data
184         x = datamat(:,2);
185         y = datamat(:,3);
186         x = x.*10^(3);
187         y = y.*10^6;
188         xdata{u} = x;
189         ydata{u} = y;
190     end;
191
192     % Because the settings for my folder are for 40x magnification and I do my
193     % 500 um channel in 20x everything needs to be doubled. -Thalia
194     if str2num(get(handles.channelsize, 'String')) >400
195         C = 2;
196     else
197         C = 1;
198     end;

```

```

199
200     if get(handles.flip, 'Value') == 1
201         K = -1;
202     else
203         K = 1;
204     end;
205
206     % Find Average values
207     xavg = K*C.*mean(cell2mat(xdata),2);
208     yavg = K*C.*mean(cell2mat(ydata),2);
209
210     % Remove zero values
211     indices = find((yavg)<=str2num(get(handles.ylower, 'String')));
212     yavg(indices) = [];
213     xavg(indices) = [];
214     indices = find((yavg)>=str2num(get(handles.yupper, 'String')));
215     yavg(indices) = [];
216     xavg(indices) = [];
217
218     [lines, ~, subs] = unique(xavg); %lines = unique values of xavg, ~ = location of those
        unique values in xavg, subs = where each value in lines is located in xavg
219     ymeanperline = accumarray(subs, yavg, [], @mean);
220
221     xavg = xavg - min(xavg);
222     indices5 = find((xavg)>=str2num(get(handles.xupper, 'String')));
223     yavg(indices5) = [];
224     xavg(indices5) = [];
225     indices6 = find((xavg)<=str2num(get(handles.xlower, 'String')));
226     yavg(indices6) = [];
227     xavg(indices6) = [];
228
229     xavg = xavg-str2num(get(handles.xlower, 'String'));
230
231     [lines, ~, subs] = unique(xavg); %lines = unique values of xavg, ~ = location of those
        unique values in xavg, subs = where each value in lines is located in xavg
232     ymeanperline = accumarray(subs, yavg, [], @mean);
233
234     height = [];
235     for v = 1:length(xavg)
236         height(v) = (j-1)*str2num(get(handles.channelsize, 'String'))/(numfolders-1);
237     end;

```

```

238
239     width = xavg;
240     velocity = yavg;
241     if get(handles.figure_check, 'Value') == 1
242         figure
243     end;
244     scatter3(width,height,velocity, '.', 'k');%3D plot
245     xlabel('Width of Channel (um)')
246     ylabel('Height of Channel (um)')
247     zlabel('Velocity (um/s)')
248     hold on
249
250     % Find and plot average
251     [lines, ~, subs] = unique(xavg); %lines = unique values of xavg, ~ = location of those
        unique values in xavg, subs = where each value in lines in located in xavg
252     ymeanperline = accumarray(subs, yavg, [], @mean);
253     height2 = [];
254     for w = 1:length(lines)
255         height2(w) = (j-1)*str2num(get(handles.channelsize, 'String'))/(numfolders-1);
256     end;
257     plot3(lines,height2,ymeanperline, 'b', 'LineWidth', 5);
258     if j ~= 1
259         if length(storelines)>length(lines)
260             net = length(storelines) - length(lines);
261             arr = zeros(net,1);
262             lines = [lines;arr];
263             height2 = [height2,transpose(arr)];
264             ymeanperline = [ymeanperline;arr];
265         end
266     end;
267     storelines(j,:) = lines;
268     storeheight(j,:) = height2;
269     storeymeanperline(j,:) = ymeanperline;
270 end;
271 handles.lines = storelines;
272 handles.height = storeheight;
273 handles.ymeanperline = storeymeanperline;
274 'Done'
275 toc
276 beep on
277 pause(1)

```

```

278 beep
279 guidata(hObject, handles);
280
281 % --- Executes on button press in savebutton.
282 function savebutton_Callback(hObject, eventdata, handles)
283 answer = {[get(handles.prefix, 'String') '_3D']};
284 myfolder = ['C:\Users\tamie\Documents\Thalia\data - thalia3\Images\' answer '\'];
285 mkdir(cell2mat(myfolder))
286
287 temp = figure;
288 set(gcf, 'Units', 'Normalized', 'OuterPosition', [0.1 0.2 0.5 0.9]);
289 copyobj(handles.axes2, temp)
290 saveas(temp, cell2mat([myfolder char(answer) '.png']));
291 saveas(temp, cell2mat([myfolder char(answer) '.fig']));
292
293 temp2 = figure;
294 lines = handles.lines;
295 height = handles.height;
296 ymeanperline = handles.ymeanperline;
297 plot3(lines, height, ymeanperline, '.', 'Color', 'k');
298 xlabel(['Width of Channel (um)'])
299 ylabel(['Height of Channel (um)'])
300 zlabel(['Velocity (um/s)'])
301 saveas(temp2, cell2mat([myfolder char(answer) '_mean' '.png']));
302 saveas(temp2, cell2mat([myfolder char(answer) '_mean' '.fig']));
303
304 temp3 = figure;
305 s = surf(lines, height, ymeanperline);
306 s.EdgeColor = 'none';
307 xlabel(['Width of Channel (um)'])
308 ylabel(['Height of Channel (um)'])
309 zlabel(['Velocity (um/s)'])
310 saveas(temp3, cell2mat([myfolder char(answer) '_surf' '.png']));
311 saveas(temp3, cell2mat([myfolder char(answer) '_surf' '.fig']));
312
313 T = [];
314 temp4 = figure;
315 for i = 1:9
316     plot(lines(i,:), ymeanperline(i,:));
317     xlabel('Width of Channel (um)')
318     ylabel('Velocity (um/s)')

```



```

319     saveas(temp4, cell2mat([myfolder char(answer) '_' num2str(i) '.png']));
320     saveas(temp4, cell2mat([myfolder char(answer) '_' num2str(i) '.fig']));
321     clf
322 end
323
324 close(temp4)
325 close(temp3)
326 close(temp2)
327 close(temp)

```

plug.m

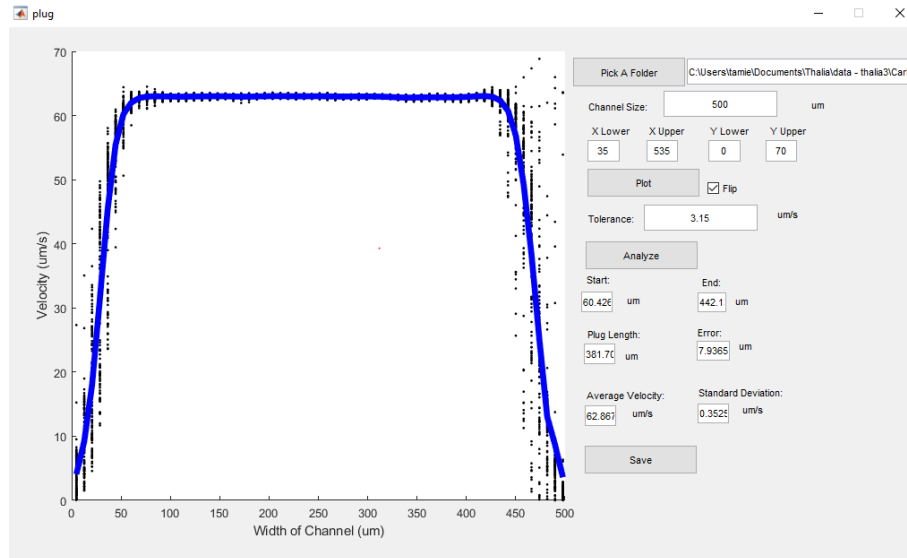


Figure A.2: plug.m GUI.

The program plug.m was used to find the average velocity of the plug region for Carbopol and PNIPAM flow profiles. The results of this data was used to form Figure 3.15.

```

1 function varargout = plug(varargin)
2 % PLUG MATLAB code for plug.fig
3 %     PLUG, by itself, creates a new PLUG or raises the existing
4 %     singleton*.
5 %
6 %     H = PLUG returns the handle to a new PLUG or the handle to
7 %     the existing singleton*.

```

```

8 %
9 %     PLUG('CALLBACK',hObject,eventData,handles,...) calls the local
10 %     function named CALLBACK in PLUG.M with the given input arguments.
11 %
12 %     PLUG('Property','Value',...) creates a new PLUG or raises the
13 %     existing singleton*. Starting from the left, property value pairs are
14 %     applied to the GUI before plug_OpeningFcn gets called. An
15 %     unrecognized property name or invalid value makes property application
16 %     stop. All inputs are passed to plug_OpeningFcn via varargin.
17 %
18 %     *See GUI Options on GUIDE's Tools menu. Choose "GUI allows only one
19 %     instance to run (singleton)".
20 %
21 % See also: GUIDE, GUIDATA, GUIHANDLES
22
23 % Edit the above text to modify the response to help plug
24
25 % Last Modified by GUIDE v2.5 30-Mar-2020 14:36:33
26
27 % Begin initialization code - DO NOT EDIT
28 gui_Singleton = 1;
29 gui_State = struct('gui_Name',       mfilename, ...
30                   'gui_Singleton',  gui_Singleton, ...
31                   'gui_OpeningFcn', @plug_OpeningFcn, ...
32                   'gui_OutputFcn',  @plug_OutputFcn, ...
33                   'gui_LayoutFcn',  [] , ...
34                   'gui_Callback',    []);
35 if nargin && ischar(varargin{1})
36     gui_State.gui_Callback = str2func(varargin{1});
37 end
38
39 if nargout
40     [varargout{1:nargout}] = gui_mainfcn(gui_State, varargin{:});
41 else
42     gui_mainfcn(gui_State, varargin{:});
43 end
44 % End initialization code - DO NOT EDIT
45
46
47 % --- Executes just before plug is made visible.
48 function plug_OpeningFcn(hObject, eventdata, handles, varargin)

```

```
49 handles.output = hObject;
50 %set(handles.folder,'String','C:\Users\tamie\Documents\Thalia\data - thalia3');
51 guidata(hObject, handles);
52
53 % --- Outputs from this function are returned to the command line.
54 function varargout = plug_OutputFcn(hObject, eventdata, handles)
55 varargout{1} = handles.output;
56
57
58 % --- Executes on button press in pickafolder.
59 function pickafolder_Callback(hObject, eventdata, handles)
60 path = uigetdir('C:\Users\thali\Documents\Research\mid plane data');
61 set(handles.folder,'String',path);
62
63 function folder_Callback(hObject, eventdata, handles)
64 set(handles.folder,'String',get(hObject,'String'));
65 guidata(hObject, handles);
66
67 % --- Executes during object creation, after setting all properties.
68 function folder_CreateFcn(hObject, eventdata, handles)
69 if ispc && isequal(get(hObject,'BackgroundColor'), get(0,'defaultUiControlBackgroundColor'))
70     set(hObject,'BackgroundColor','white');
71 end
72
73 function channelsize_Callback(hObject, eventdata, handles)
74 set(handles.channelsize,'String',get(hObject,'String'));
75 guidata(hObject, handles);
76
77 % --- Executes during object creation, after setting all properties.
78 function channelsize_CreateFcn(hObject, eventdata, handles)
79 if ispc && isequal(get(hObject,'BackgroundColor'), get(0,'defaultUiControlBackgroundColor'))
80     set(hObject,'BackgroundColor','white');
81 end
82
83 function xlower_Callback(hObject, eventdata, handles)
84 set(handles.xlower, 'String', get(hObject, 'String'));
85 guidata(hObject, handles);
86
87 % --- Executes during object creation, after setting all properties.
88 function xlower_CreateFcn(hObject, eventdata, handles)
89 if ispc && isequal(get(hObject,'BackgroundColor'), get(0,'defaultUiControlBackgroundColor'))
```

```

90     set(hObject,'BackgroundColor','white');
91 end
92
93 function xupper_Callback(hObject, eventdata, handles)
94 set(handles.xupper, 'String', get(hObject, 'String'));
95 guidata(hObject, handles);
96
97 % --- Executes during object creation, after setting all properties.
98 function xupper_CreateFcn(hObject, eventdata, handles)
99 if ispc && isequal(get(hObject,'BackgroundColor'), get(0,'defaultUicontrolBackgroundColor'))
100     set(hObject,'BackgroundColor','white');
101 end
102
103 function ylower_Callback(hObject, eventdata, handles)
104 set(handles.ylower, 'String', get(hObject, 'String'));
105 guidata(hObject, handles);
106
107 % --- Executes during object creation, after setting all properties.
108 function ylower_CreateFcn(hObject, eventdata, handles)
109 if ispc && isequal(get(hObject,'BackgroundColor'), get(0,'defaultUicontrolBackgroundColor'))
110     set(hObject,'BackgroundColor','white');
111 end
112
113 function yupper_Callback(hObject, eventdata, handles)
114 set(handles.yupper, 'String', get(hObject, 'String'));
115 guidata(hObject, handles);
116
117 % --- Executes during object creation, after setting all properties.
118 function yupper_CreateFcn(hObject, eventdata, handles)
119 if ispc && isequal(get(hObject,'BackgroundColor'), get(0,'defaultUicontrolBackgroundColor'))
120     set(hObject,'BackgroundColor','white');
121 end
122
123 % --- Executes on button press in plotbutton.
124 function plotbutton_Callback(hObject, eventdata, handles)
125 cla
126 path = get(handles.folder, 'String');
127 dirinfo = dir(path);
128 count = 1;
129 for K = 3: length(dirinfo)
130     thisdir = dirinfo(K).name;

```

```
131     subdirname{count} = dir(fullfile(path, thisdir));
132     files(count,:) = {subdirname{1}.name};
133     count = count + 1;
134 end;
135
136 [numfolders numfiles] = size(files);
137
138 for u = 1:numfiles %typically 9
139     fullfilename = [path '\' files{u}];
140     % Read file in as a series of strings
141     fid = fopen(fullfilename, 'rb');
142     strings = textscan(fid, '%s', 'Delimiter', '');
143     fclose(fid);
144
145     % Replace all commas with decimal points
146     decimal_strings = regexp(strings{1}, ',', '.');
147
148     % Convert to doubles and join all rows together
149     data = cellfun(@str2num, decimal_strings, 'uni', 0);
150     data = cat(1, data{:});
151
152     % Convert to matrix
153     datamat = cell2mat({data});
154
155     % Get x and y data
156     x = datamat(:,2);
157     y = datamat(:,3);
158     x = x.*10^(3);
159     y = y.*10^6;
160     xdata{u} = x;
161     ydata{u} = y;
162 end;
163
164 % Because the settings for my folder are for 40x magnification and I do my
165 % 500 um channel in 20x everything needs to be doubled. -Thalia
166 if str2num(get(handles.channelsize, 'String')) >400
167     C = 2;
168 else
169     C = 1;
170 end;
171
```

```

172 if get(handles.flip, 'Value') == 1
173     K = -1;
174 else
175     K = 1;
176 end;
177
178 % Find Average values
179 xavg = K*C.*mean(cell2mat(xdata),2);
180 yavg = K*C.*mean(cell2mat(ydata),2);
181
182 % Remove zero values
183 indices = find((yavg)<=str2num(get(handles.ylower, 'String')));
184 yavg(indices) = [];
185 xavg(indices) = [];
186 indices = find((yavg)>=str2num(get(handles.yupper, 'String')));
187 yavg(indices) = [];
188 xavg(indices) = [];
189
190 [lines, ~, subs] = unique(xavg); %lines = unique values of xavg, ~ = location of those unique
    values in xavg, subs = where each value in lines is located in xavg
191 ymeanperline = accumarray(subs, yavg, [], @mean);
192
193 xavg = xavg - min(xavg);
194 indices5 = find((xavg)>=str2num(get(handles.xupper, 'String')));
195 yavg(indices5) = [];
196 xavg(indices5) = [];
197 indices6 = find((xavg)<=str2num(get(handles.xlower, 'String')));
198 yavg(indices6) = [];
199 xavg(indices6) = [];
200
201 xavg = xavg-str2num(get(handles.xlower, 'String'));
202
203 width = xavg;
204 velocity = yavg;
205
206 scatter(width,velocity,','.','k');%3D plot
207 xlabel('Width of Channel (um)')
208 ylabel('Velocity (um/s)')
209 hold on
210
211 % Find and plot average

```

```

212 [lines, ~, subs] = unique(xavg); %lines = unique values of xavg, ~ = location of those unique
      values in xavg, subs = where each value in lines is located in xavg
213 ymeanperline = accumarray(subs, yavg, [], @mean);
214 plot(lines, ymeanperline, 'b', 'LineWidth', 5);
215 hold off
216 handles.data = [ymeanperline lines];
217 'Plotted'
218 guidata(hObject, handles);
219
220 % --- Executes on button press in flip.
221 function flip_Callback(hObject, eventdata, handles)
222
223 % --- Executes on button press in tolerance.
224 function tolerance_Callback(hObject, eventdata, handles)
225 set(handles.tolerance, 'String', get(hObject, 'String'));
226 guidata(hObject, handles);
227
228 % --- Executes during object creation, after setting all properties.
229 function tolerance_CreateFcn(hObject, eventdata, handles)
230 if ispc && isequal(get(hObject, 'BackgroundColor'), get(0, 'defaultUicontrolBackgroundColor'))
231     set(hObject, 'BackgroundColor', 'white');
232 end
233
234 % --- Executes on button press in analyze.
235 function analyze_Callback(hObject, eventdata, handles)
236 channelsize = str2num(get(handles.channelsize, 'String'));
237 data = handles.data;
238 ydata = data(:,1);
239 xdata = data(:,2);
240 tol = str2num(get(handles.tolerance, 'String'));
241 count = 0;
242 for i = 2:length(ydata)
243     if abs(ydata(i,1)-ydata(i-1,1)) < tol
244         count = count + 1;
245         result(:,count) = [ydata(i,1) xdata(i,1)];
246     end
247 end
248 result
249 len = length(result);
250 set(handles.startnum, 'String', result(2,1));
251 set(handles.endnum, 'String', result(2,len));

```

```

252 avg = mean(result(1,:));
253 stdev = std(result(1,:));
254 pluglen = result(2,len)-result(2,1);
255 err = channelsize/length(ydata);
256 set(handles.velocity, 'String', avg);
257 set(handles.std, 'String', stdev);
258 set(handles.pluglen, 'String', pluglen);
259 set(handles.err, 'String', err);
260 startnum = result(2,1); %Where my program determined the start of the plug to be
261 endnum = result(2,len);
262 xplug = xdata;
263 yplug = ydata;
264 indstart = find(xplug<startnum);
265 xplug(indstart) = [];
266 yplug(indstart) = [];
267 indend = find(xplug>endnum);
268 xplug(indend) = [];
269 yplug(indend) = [];
270 f = fit(xplug,yplug,'poly1')
271 %figure(1)
272 hold on
273 h = plot(f,xplug,yplug)
274 set(h,'LineWidth',2)
275 xlabel(['Width of Channel (' char(181) 'm)'])
276 ylabel(['Velocity (' char(181) 'm/s)'])
277 b = gca; legend(b,'off');
278 hold off
279
280 count2 = 0;
281 standev = std(yplug);
282 indend = find(xdata>endnum);
283 m = 2;
284 n = length(xplug);
285 result2=[];
286 for i = m:n
287     if abs(ydata(i,1)-ydata(i-1,1)) > 0.1*standev
288         count2 = count2 + 1;
289         result2(count2,:) = [ydata(i,1);xdata(i,1)];
290     end
291 end
292 result2

```



```
293 'Analyzed'
294 guidata(hObject,handles);
295
296 function startnum_Callback(hObject, eventdata, handles)
297 set(handles.startnum, 'String', get(hObject, 'String'));
298 guidata(hObject, handles);
299
300 % --- Executes during object creation, after setting all properties.
301 function startnum_CreateFcn(hObject, eventdata, handles)
302 if ispc && isequal(get(hObject,'BackgroundColor'), get(0,'defaultUicontrolBackgroundColor'))
303     set(hObject,'BackgroundColor','white');
304 end
305
306 function endnum_Callback(hObject, eventdata, handles)
307 set(handles.endnum, 'String', get(hObject, 'String'));
308 guidata(hObject, handles);
309
310 % --- Executes during object creation, after setting all properties.
311 function endnum_CreateFcn(hObject, eventdata, handles)
312 if ispc && isequal(get(hObject,'BackgroundColor'), get(0,'defaultUicontrolBackgroundColor'))
313     set(hObject,'BackgroundColor','white');
314 end
315
316 function pluglen_Callback(hObject, eventdata, handles)
317 set(handles.pluglen, 'String', get(hObject, 'String'));
318 guidata(hObject, handles);
319
320 % --- Executes during object creation, after setting all properties.
321 function pluglen_CreateFcn(hObject, eventdata, handles)
322 if ispc && isequal(get(hObject,'BackgroundColor'), get(0,'defaultUicontrolBackgroundColor'))
323     set(hObject,'BackgroundColor','white');
324 end
325
326 function err_Callback(hObject, eventdata, handles)
327 set(handles.err, 'String', get(hObject, 'String'));
328 guidata(hObject, handles);
329
330 % --- Executes during object creation, after setting all properties.
331 function err_CreateFcn(hObject, eventdata, handles)
332 if ispc && isequal(get(hObject,'BackgroundColor'), get(0,'defaultUicontrolBackgroundColor'))
333     set(hObject,'BackgroundColor','white');
```

```

334 end
335
336 function velocity_Callback(hObject, eventdata, handles)
337 set(handles.velocity, 'String', get(hObject, 'String'));
338 guidata(hObject, handles);
339
340 % --- Executes during object creation, after setting all properties.
341 function velocity_CreateFcn(hObject, eventdata, handles)
342 if ispc && isequal(get(hObject,'BackgroundColor'), get(0,'defaultUicontrolBackgroundColor'))
343     set(hObject,'BackgroundColor','white');
344 end
345
346 function std_Callback(hObject, eventdata, handles)
347 set(handles.std, 'String', get(hObject,'String'));
348 guidata(hObject, handles);
349
350 % --- Executes during object creation, after setting all properties.
351 function std_CreateFcn(hObject, eventdata, handles)
352 if ispc && isequal(get(hObject,'BackgroundColor'), get(0,'defaultUicontrolBackgroundColor'))
353     set(hObject,'BackgroundColor','white');
354 end
355
356 % --- Executes on button press in savebutton.
357 function savebutton_Callback(hObject, eventdata, handles)
358 temp = figure;
359 set(gcf, 'Units', 'Normalized', 'OuterPosition', [0.1 0.2 0.9 0.9]);
360 copyobj(handles.axes2,temp)
361 prompt = {'Enter figure name'};
362 dlgtitle = 'Figure Name';
363 dims = [1 35];
364 answer = inputdlg(prompt,dlgtitle,dims);
365 saveas(temp, [char(answer) '.png']);
366 close(temp)
367 % endnum = str2num(get(handles.endnum, 'String'));
368 % startnum = str2num(get(handles.startnum, 'String'));
369 % pluglen = endnum-startnum;
370 % data = handles.data;
371 % ydata = data(:,1);
372 % xdata = data(:,2);
373 % indstart = find(xdata<startnum);
374 % xdata(indstart) = [];

```

```
375 % ydata(indstart) = [];
376 % indend = find(xdata>endnum);
377 % xdata(indend) = [];
378 % ydata(indend) = [];
379 % velocity = mean(ydata)
380 % set(handles.velocity, 'String', velocity);
381 % set(handles.pluglen, 'String', pluglen);
382 % T = [{get(handles.folder, 'String')}, velocity, ...
383 %      get(handles.std, 'String'), pluglen, ...
384 %      get(handles.err, 'String')];
385 % xlsappend('C:\Users\thali\Documents\Research\plug results.xlsx', T, 1);
386 'Saved'
```

Curriculum Vitae

Name: Thalia Magyar

**Post-Secondary
Education and
Degrees:** Acadia University
Wolfville, NS
2014 - 2018 B.Sc.

The University of Western Ontario
London, ON
2018 - 2020 M.Sc.

**Honours and
Awards:** Western Graduate Research Scholarship • Sept. 2018 – Aug. 2020
Pre-Graduate Research Scholarship • May – Aug. 2018
Honours Summer Research Award • May – Aug. 2017
Canadian Frailty Network Summer Student Award • May – Aug. 2016

**Related Work
Experience:** Teaching Assistant
The University of Western Ontario
2018 - 2020

Teaching Assistant
Acadia University
2015-2018

Conference Presentations:

Viscoplastic Fluids 8: From Theory to Application • Cambridge, UK, 2019
Poster and short oral presentation
Complex Fluids in Microfluidic Channels

Atlantic Universities Physics and Astronomy Conference • Charlottetown, PEI, 2017
Oral presentation

Biomarker Identification for Dementia and Brain Tumour Tissue Characterization with Magnetic Resonance Imaging

Canadian Frailty Network National Conference • Toronto, ON, 2017

Poster presentation

Biomarker Identification for Dementia and Brain Tumour Tissue Characterization with Magnetic Resonance Imaging

Acadia Research and Innovation Conference • Wolfville, NS, 2017

Oral presentation

Biomarker Identification for Dementia and Brain Tumour Tissue Characterization with Magnetic Resonance Imaging

Medical Physics Undergraduate Summer Student Symposium • Winnipeg, MB, 2017

Oral presentation

Biomarker Identification for Dementia and Brain Tumour Tissue Characterization with Magnetic Resonance Imaging

Women In Physics Canada Conference • Saskatoon, SK, 2017

Oral presentation

Biomarker Identification for Dementia and Brain Tumour Tissue Characterization with Magnetic Resonance Imaging

Publications:

Charge density waves in the low-dimensional compounds $A_x\text{Nb}_3\text{Te}_4$ with $A = \text{Ag}, \text{Ga}, \text{Zn}$, $0 < x < 1$.

B.Sc.H. Thesis dissertation with Acadia University, 2018.

Birdcage volume coils and magnetic resonance imaging: a simple experiment for students.

Journal of biological engineering, 11(1), 1-7.

Dwight E. Vincent, Tianhao Wang, Thalia A. K. Magyar, Peni I. Jacob, Richard Buist, Melanie Martin.

Ex vivo tissue imaging of human glioblastoma using a small bore 7T MRI and correlation with digital pathology and proteomics profiling by multiplex tissue immunoblotting.

Medical Imaging 2017: Biomedical Applications in Molecular, Structural, and Functional Imaging. Vol. 10137. International Society for Optics and Photonics, 2017.

Kant M. Matsuda, Ana Lopes-Calças, Thalia Magyar, Zoe O'Brien-Moran, Richard Buist, Melanie Martin.